PHYSICAL REVIEW D **80,** 083502 (2009)

DAMA/LIBRA data and leptonically interacting dark matter

Joachim Kopp,[1,*] Viviana Niro,[1,†] Thomas Schwetz,[1,‡] and Jure Zupan[2,§]

[1]*Max-Planck-Institute for Nuclear Physics, PO Box 103980, 69029 Heidelberg, Germany*

[2]*Theory Division, Physics Department, CERN, CH-1211 Geneva 23, Switzerland*

(Received 27 July 2009; published 2 October 2009)

We consider the hypothesis that dark matter (DM) has tree-level interactions only with leptons. Such a framework, where DM recoils against electrons bound in atoms, has been proposed as an explanation for the annually modulated scintillation signal in DAMA/LIBRA data versus the absence of a signal for nuclear recoils in experiments like CDMS or XENON10. However, even in such a leptophilic DM scenario there are loop-induced DM-hadron interactions, where photons emitted from virtual leptons couple to the charge of a nucleus. Using a general effective field theory approach we show that, if such an interaction is induced at one- or two-loop level, then DM-nucleus scattering dominates over DM-electron scattering. This is because the latter is suppressed by the bound state wave function. One obtains a situation similar to standard DM-nucleus scattering analyses with considerable tension between the results of DAMA and CDMS/XENON10. This conclusion does not apply in the case of pseudoscalar or axial-vector coupling between DM and leptons, where the loop diagrams vanish. In this case the explanation of the DAMA signal in terms of DM-electron scattering is strongly disfavored by the spectral shape of the signal. Furthermore, if DM can annihilate into neutrinos or tau leptons, the required cross sections are excluded by many orders of magnitude using the Super-Kamiokande bound on neutrinos from DM annihilations in the Sun.

DOI: 10.1103/PhysRevD.80.083502 PACS numbers: 95.35.+d

I. INTRODUCTION

The DAMA Collaboration provided strong evidence for an annually modulated signal in the scintillation light from sodium iodine detectors. The combined data from DAMA/NaI [1] (7 annual cycles) and DAMA/LIBRA [2] (4 annual cycles) with a total exposure of 0.82 ton yr show a modulation signal with 8.2σ significance. The phase of this modulation agrees with the assumption that the signal is due to the scattering of weakly interacting massive particles (WIMPs) forming the dark matter (DM) halo of our Galaxy.

However, many interpretations of this signal in terms of DM scattering are in conflict with constraints from other DM direct detection experiments. Spin-independent elastic WIMP-nucleon scattering accounting for the DAMA modulation is tightly constrained by bounds from several experiments, most notably from CDMS [3] and XENON10 [4]. While conventional WIMPs with masses $m_\chi \gtrsim 50$ GeV are excluded by many orders of magnitude, light WIMPs with $\lesssim 10$ GeV masses might be marginally compatible with the constraints, see, e.g. [5–12] for recent studies. Spin-dependent couplings to protons can account for the DAMA signal without being in conflict with CDMS and XENON10, but in this case strong constraints from COUPP [13], KIMS [14], and PICASSO [15], as well as (somewhat model dependent) bounds from Super-Kamiokande [16] searches for neutrinos from DM annihilations inside the Sun apply [11,17]. Inelastic scattering of a DM particle to a nearly degenerate excited state has been proposed in [18]; see [19–23] for recent analyses, though also in this case tight constraints apply, in particular, from CRESST-II [24] and ZEPLIN-II [25]. Other proposals include mirror world DM [26] or DM with electric or magnetic dipole moments [27].

In this work we consider the hypothesis that the DM sector has no direct couplings to quarks, only to leptons, in particular, the electrons. While electronic events will contribute to the scintillation light signal in DAMA, most other DM experiments like CDMS or XENON reject pure electron events by aiming at a (close to) background free search for nuclear recoils. DM scattering off electrons at rest cannot provide enough energy to be seen in a detector, however, exploiting the tail of the momentum distribution of electrons bound in an atom may lead to a scintillation light signal in DAMA of the order of a few keV [28]. The signal in direct detection experiments from DM-electron scattering has been considered recently also in Ref. [29]. An affinity of DM to leptons might also be motivated by recent cosmic ray anomalies [30–32] observed in elec-

*jkoppATmpi-hd.mpg.de
†niroATmpi-hd.mpg.de
‡schwetzATmpi-hd.mpg.de
§On leave of absence from Faculty of Mathematics and Physics, University of Ljubljana, Jadranska 19, 1000 Ljubljana, Slovenia, and Josef Stefan Institute, Jamova 39, 1000 Ljubljana, Slovenia.
jure.zupanATcern.ch

trons/positrons, but not in antiprotons. A simple model for ''leptophilic'' DM has been presented in Ref. [33]; see in this context, for example, also [34,35] and references therein.

In the following we will use effective field theory to perform a model independent analysis. We will consider all possible Lorentz structures for the effective DM-electron interaction and show that in many cases a DM-quark interaction is induced at one- or two-loop level by photon exchange. In these cases the loop-induced DM-nucleon scattering always dominates, since the DM-electron scattering cross section is suppressed by the momentum wave function. This reintroduces the tension between DAMA and other searches. We identify only one possible Lorentz structure, the axial-vector type coupling, where DM-electron scattering dominates and the scattering cross section is not additionally suppressed by small quantities. Taking special care of the kinematics in the DM scattering off bound electrons, we show that in this case the fit to the DAMA event spectrum is very bad. Super-Kamiokande constraints on neutrinos from DM annihilations inside the Sun also disfavor this possibility. Our results thus suggest that leptonically interacting DM is not a viable explanation of the DAMA annual modulation signal.

The plan of the paper is as follows. In Sec. II we introduce the effective Lagrangian for DM-lepton interactions, discuss three possible experimental signatures of leptophilic DM, and estimate their relative sizes. In Sec. III we discuss all the possible Lorentz structures and the implications for tree-level interactions with electrons as well as loop-induced DM-nucleus interactions. In Sec. IV the event rates in direct detection experiments are calculated, while Sec. V contains the numerical results for two representative examples, namely, vectorlike couplings, where the count rate is dominated by loop-induced WIMP-nucleus scattering (Sec. V A), and axial-vector coupling, where no loop contribution is present and WIMP-electron scattering off bound electrons dominates (Sec. V B). In Sec. VI we show that the cross sections required in the axial-vector case are ruled out by Super-Kamiokande constraints assuming that DM annihilations in the Sun produce neutrinos; we point out the importance of the nonzero temperature of the electrons in the Sun. We summarize our results in Sec. VII. Technical details and supplementary information is given in Appendixes A, B, C, and D.

II. LEPTONICALLY INTERACTING DARK MATTER

A. Effective dark matter interactions

The goal of our study is a model independent analysis under the assumption that the DM particle χ couples directly only to leptons but not to quarks. The appropriate description is in terms of effective interactions. Let us first focus on the case of fermionic DM. The most general dimension six four-Fermi effective interactions are then, shown pictorially also in Fig. 1 (right diagram),

$$\mathcal{L}_{\text{eff}} = \sum_i G(\bar{\chi}\Gamma^i_\chi \chi)(\bar{\ell}\Gamma^i_\ell \ell) \quad \text{with} \quad G = \frac{1}{\Lambda^2}, \tag{1}$$

where Λ is the cutoff scale for the effective field theory description, while the sum is over different Lorentz structures. A complete set consists of scalar (S), pseudoscalar (P), vector (V), axial-vector (A), tensor (T), and axial-tensor (AT) currents. The four-Fermi operators can thus be classified to be of

$$\begin{aligned}
&\text{scalar type: } \Gamma_\chi = c_S^\chi + ic_P^\chi\gamma_5, && \Gamma_\ell = c_S^\ell + ic_P^\ell\gamma_5,\\
&\text{vector type: } \Gamma_\chi^\mu = (c_V^\chi + c_A^\chi\gamma_5)\gamma^\mu, &&\\
&\qquad\qquad \Gamma_{\ell\mu} = (c_V^\ell + c_A^\ell\gamma_5)\gamma_\mu, &&\\
&\text{tensor type: } \Gamma_\chi^{\mu\nu} = (c_T + ic_{AT}\gamma_5)\sigma^{\mu\nu}, && \Gamma_{\ell\mu\nu} = \sigma_{\mu\nu},
\end{aligned} \tag{2}$$

where $\sigma_{\mu\nu} = \frac{i}{2}[\gamma_\mu, \gamma_\nu]$.[1] If DM is a Majorana particle, vector and tensorlike interactions are forbidden, i.e., $c_V^\chi = c_T^\chi = c_{AT}^\chi = 0$.

In our work we do not rely on any specific realization of the effective interaction. The simplest example would just be assuming that the interaction is induced by the exchange of an intermediate particle whose mass is much larger than the recoil momenta that are of order of a few MeV. The intermediate particle can then be integrated out leaving an effective point interaction. Let us look at the χ-lepton interaction mediated by a scalar field ϕ, shown in Fig. 1. It gives an amplitude

$$\begin{aligned}
&ig_S^\chi(\bar{u}_\chi u_\chi)\frac{i}{q^2 - m_\phi^2 + i\epsilon}ig_S^\ell(\bar{u}_\ell u_\ell)\\
&\quad\rightarrow i\frac{g_S^\chi g_S^\ell}{m_\phi^2}(\bar{u}_\chi u_\chi)(\bar{u}_\ell u_\ell),
\end{aligned} \tag{3}$$

where on the right-hand side we have neglected the momentum transfer $q^2 = (p' - p)^2 \ll m_\phi^2$. The same amplitude is obtained from a local operator $(\bar{\chi}\chi)(\bar{\ell}\ell)$ with a Wilson coefficient $g_S^\chi g_S^\ell/m_\phi^2$ [in the notation used in Eqs. (1) and (2) we have $c_S^\chi = g_S^\chi$, $c_S^\ell = g_S^\ell$, and $\Lambda = m_\phi$].

In the case of scalar DM, at lowest order there is only one dimension five operator. The effective Lagrangian is given by

$$\mathcal{L}_{\text{eff}} = G_5(\chi^\dagger\chi)[\bar{\ell}(d_S + id_P\gamma_5)\ell] \quad \text{with} \quad G_5 = \frac{1}{\Lambda}. \tag{4}$$

[1]The relation $\sigma^{\mu\nu}\gamma_5 = \frac{i}{2}\epsilon^{\mu\nu\alpha\beta}\sigma_{\alpha\beta}$ implies that the $AT \otimes AT$ coupling is equivalent to $T \otimes T$, and $T \otimes AT = AT \otimes T$.

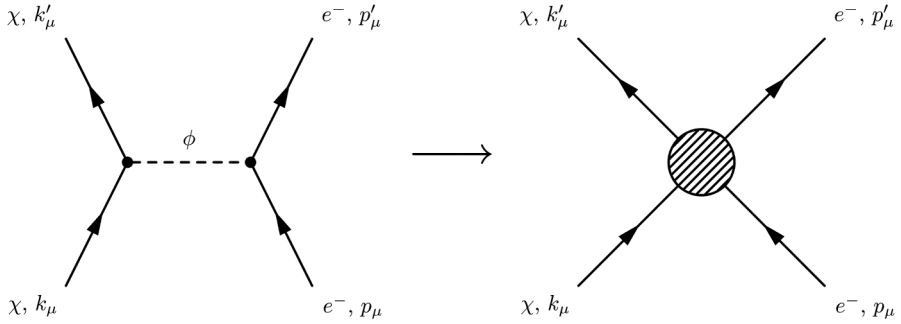

FIG. 1. Example for generating an effective local DM-electron interaction vertex (right diagram) as used in our analysis by the exchange of a heavy intermediate particle ϕ (left diagram).

B. Signals in direct detection experiments

Let us now discuss the signals that arise when a leptophilic DM particle interacts in a detector. One can distinguish the following types of signals (see also [29]):

(1) *WIMP-electron scattering* (WES): The whole recoil is absorbed by the electron that is then kicked out of the atom to which it was bound.

(2) *WIMP-atom scattering* (WAS): The electron on which the DM particle scatters remains bound and the recoil is taken up by the whole atom. The process can either be elastic (el-WAS) in which case the electron wave function remains the same, or inelastic (ie-WAS), in which case the electron is excited to an outer shell.

(3) Loop-induced *WIMP-nucleus scattering* (WNS): Although per assumption DM couples only to leptons at tree level, an interaction with quarks is induced at loop level, by coupling a photon to virtual leptons, see Fig. 2. This will lead to scattering of the DM particle off nuclei.

WES produces a prompt electron and possibly additional Auger electrons or x rays. This leads to a signal in scintillation detectors such as DAMA, but is rejected in nuclear recoil experiments like CDMS and XENON. If WES was the dominant mechanism, it might be possible to explain both the DAMA signal and the absence of the signal in CDMS and XENON. In the other two cases, WAS and WNS, the signal consists of a scattered nucleus and shows up in all direct detection experiments searching for

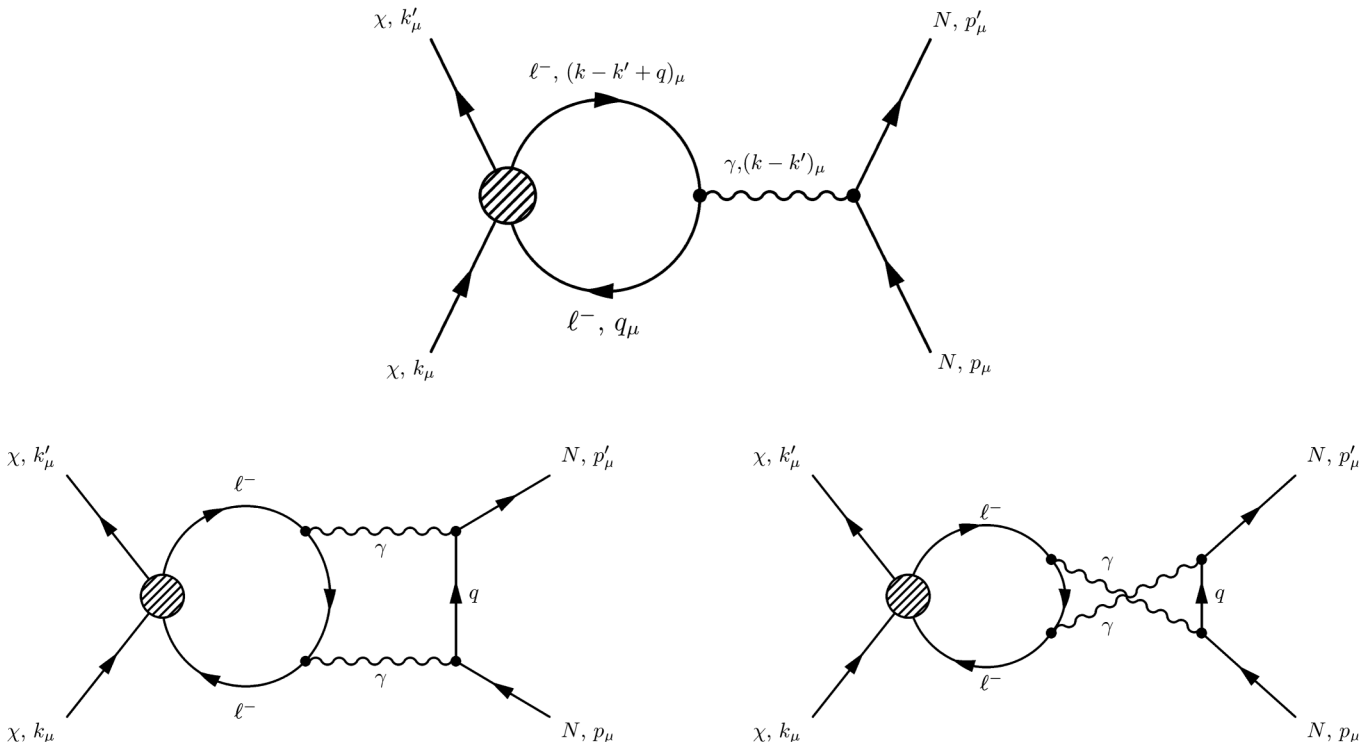

FIG. 2. DM-nucleus interaction induced by a charged lepton loop and photon exchange at one loop (top) and two loop (bottom).

DM nuclear recoils. If WAS or WNS was the dominant signal, then the leptophilic nature of DM would not help to resolve the tension between DAMA and the remaining experiments. In the following we will first give rough estimates for the relative sizes of these three signal types for different DM-lepton effective interactions, while giving a more detailed calculation of the event rates later in Sec. IV and Appendix B.

The event rate in direct detection experiments is proportional to the differential cross section $d\sigma/dE_d$, where

$$E_d = E_\chi - E'_\chi, \tag{5}$$

is the energy deposited by the WIMP in the detector. The DAMA annual modulation signal is observed at $E_d \simeq 3$ keV. Also for other direct detection experiments typical values are in the few to tens of keV range. As we will see in Sec. IV and Appendix B, just from kinematics the cross section is proportional to

$$\frac{d\sigma}{dE_d} \propto G^2 m_e (G^2 m_N) \quad \text{for WES (WAS, WNS)}, \tag{6}$$

where G is defined in Eq. (1) and m_e (m_N) is the electron (nucleus) mass. This suppresses the WES induced event rate by a factor m_e/m_N with respect to WAS and WNS.

In order for WES to deposit ~keV energy in the detector, the electron that a WIMP scatters off has to have quite a high momentum. Indeed, the maximal detectable energy from DM scattering on electrons at rest is $2m_e v^2$, with typical DM velocities of $v \sim 10^{-3}c$. Hence, the maximal detectable energy is of order eV, far too low to be relevant for the DAMA signal at few keV. Therefore, one has to explore the scattering off bound electrons with non-negligible momentum [28]. In this case the energy transfer to the detector is $E_d \sim \mathcal{O}(pv)$, and an electron momentum $p \sim$ MeV is required to obtain $E_d \sim$ keV. Since electrons are bound in the atom, there is a finite yet small probability that it carries such high momentum. The detailed calculations below will show that the suppression factor from the wave function is given by the expression

$$\epsilon_{\mathrm{WES}} = \sqrt{2m_e(E_d - E_B)}(2l+1)\int \frac{dp\,p}{(2\pi)^3}|\chi_{nl}(p)|^2 \sim 10^{-6}. \tag{7}$$

The integral is over MeV momenta, while $\chi_{nl}(p)$ is the momentum wave function of the shell nl with the binding energy E_B. Some wave functions are shown in Fig. 3, which we have used to obtain the numerical estimate for $\epsilon_{\mathrm{WES}} \sim 10^{-6}$ given above.

Similarly, WAS is also suppressed by the overlap of atomic wave functions of the initial and final states of the electron:

$$\epsilon_{\mathrm{WAS}} = \sum |\langle n'l'm'|e^{i(\mathbf{k}-\mathbf{k}')\mathbf{x}}|nlm\rangle|^2 \sim 10^{-19}, \tag{8}$$

where the numerical estimate follows from Fig. 10 for a momentum transfer of $|\mathbf{k} - \mathbf{k}'| = \sqrt{2m_N(E_d - \delta E_B)} \sim 10$ MeV.

Loop-induced WNS does not suffer from any wave function suppression, but instead carries a loop factor. At 1-loop the suppression is of order $(\alpha_{\mathrm{em}} Z/\pi)^2$, with Z being the charge number of the nucleus. Combining this with Eqs. (6)–(8), we obtain the following rough estimate for the ratios of WAS, WES, and WNS induced event rates (neglecting order-one factors but also possible different v dependences):

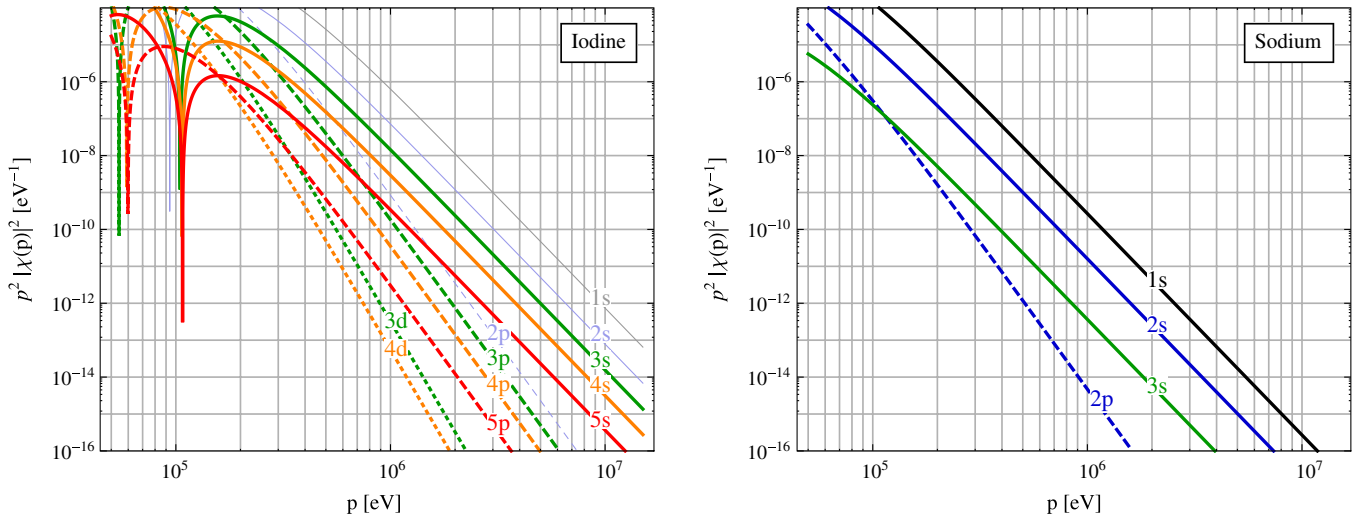

FIG. 3 (color online). Momentum space wave functions of iodine and sodium. Solid colored curves correspond to shells that contribute to WES in DAMA, while thin light curves are for shells that are not accessible in DAMA.

$$R^{\rm WAS}:R^{\rm WES}:R^{\rm WNS} \sim \epsilon_{\rm WAS}:\epsilon_{\rm WES}\frac{m_e}{m_N}:\left(\frac{\alpha_{\rm em}Z}{\pi}\right)^2 \sim 10^{-17}:10^{-10}:1, \quad (9)$$

where in the last step we used $m_N = 100$ GeV and $Z = 53$.

We conclude that whenever a loop-induced cross section is present it will dominate the rate in direct detection experiments. This holds for 1-loop as well as 2-loop cross sections, since the latter will be suppressed by another factor $(\alpha_{\rm em}Z/\pi)^2 \simeq 5\times 10^{-6}Z^2$ relative to 1-loop, and hence they are still much larger than the WES contribution. As we will show in the next section for axial-vectorlike DM-lepton coupling no loop will be induced. Therefore, in this case the signal in DAMA will be dominated by WES. Then, WAS is still irrelevant for DAMA, but since WES will not contribute to the rate in CDMS and XENON, WAS might in principle lead to a signal in those experiments.

III. DM-ELECTRON SCATTERING VERSUS LOOP-INDUCED NUCLEAR RECOIL

Having estimated the strong hierarchy among the WAS, WES, and WNS signals in the previous section, we now discuss which type of signal is present for a given Lorentz structure of the effective DM-lepton vertex, Eqs. (2) and (4).

A. DM scattering on electrons

Let us start by investigating DM scattering on electrons, relevant for WES and WAS. To simplify the discussion we consider χ scattering on electrons at rest. This will enable us to see for which types of Lorentz structures in the effective DM-lepton Lagrangian, Eq. (1), this interaction is relevant. We defer the complications introduced by the fact that electrons are actually bound in atoms to Sec. IV and Appendix B.

We consider a DM particle χ of mass m_χ scattering elastically on a free electron at rest, assuming that all the particles are nonrelativistic. The scattering cross sections for fermionic DM are then

$$\text{scalar type: } \sigma = \sigma^0_{\chi e}\left\{(c^\chi_S c^e_S)^2 + \left[(c^\chi_S c^e_P)^2 + (c^\chi_P c^e_S)^2\frac{m_e^2}{m_\chi^2}\right]\times\frac{v^2}{2} + \frac{(c^\chi_P c^e_P)^2}{3}\frac{m_e^2}{m_\chi^2}v^4\right\}, \quad (10)$$

$$\text{vector type: } \sigma = \sigma^0_{\chi e}\left\{(c^\chi_V c^e_V)^2 + 3(c^\chi_A c^e_A)^2 + [(c^\chi_V c^e_A)^2 + 3(c^\chi_A c^e_V)^2]\frac{v^2}{2}\right\}, \quad (11)$$

$$\text{tensor type: } \sigma = \sigma^0_{\chi e}\{12c_T^2 + 6c_{AT}^2 v^2\}. \quad (12)$$

In the above expressions there are two suppression factors, the DM velocity in our halo $v \sim 10^{-3}c$ and the ratio m_e/m_χ. The cross section for each Lorentz structure is given to leading order in these expansion parameters. Up to the velocity or electron mass suppression the typical size of the scattering cross section is

$$\sigma^0_{\chi e} \equiv \frac{G^2 m_e^2}{\pi} = \frac{m_e^2}{\pi\Lambda^4} \approx 3.1\times 10^{-39}\ {\rm cm}^2\left(\frac{\Lambda}{10\ {\rm GeV}}\right)^{-4}. \quad (13)$$

For scalar DM the χe scattering cross section is induced by the dimension 5 operator, Eq. (4), giving

$$\sigma = \sigma^0_{\chi e,5}\left(d_S^2 + \frac{d_P^2}{2}v^2\right), \quad (14)$$

with

$$\sigma^0_{\chi e,5} \equiv \frac{G_5^2}{4\pi}\frac{m_e^2}{m_\chi^2} = \frac{1}{4\pi\Lambda^2}\frac{m_e^2}{m_\chi^2} = 7.7\times 10^{-42}\ {\rm cm}^2\left(\frac{\Lambda}{10\ {\rm GeV}}\right)^{-2}\left(\frac{m_\chi}{100\ {\rm GeV}}\right)^{-2}. \quad (15)$$

Compared to fermionic DM two powers of Λ are replaced by m_χ which typically is larger than Λ. The scalar DM scattering cross section is thus further suppressed compared to the fermionic case for given Λ. The results of Eqs. (10)–(12) and (14) are summarized in the middle column of Table I.

TABLE I. Scattering cross section suppression by small parameters for DM-electron scattering and loop-induced DM-nucleon scattering for all possible Lorentz structures. Here, $v \sim 10^{-3}$ is the DM velocity, $r_e = m_e/m_\chi$, and $q_\ell = m_\ell/m_N$ ($\ell = e$, μ, τ). The reference cross sections $\sigma^0_{\chi e}$, $\sigma^0_{\chi e,5}$, $\sigma^1_{\chi N}$, and $\sigma^1_{\chi N,5}$ are defined in Eqs. (13), (15), and (26). The couplings c^χ, c^ℓ, and d have been set to 1. The entries for $\chi N \to \chi N$ are orders of magnitude estimates.

	Fermionic DM		
$\Gamma_\chi \otimes \Gamma_\ell$	$\sigma(\chi e \to \chi e)/\sigma^0_{\chi e}$	$\sigma(\chi N \to \chi N)/\sigma^1_{\chi N}$	
$S \otimes S$	1	$\alpha_{\rm em}^2$	(2 loop)
$S \otimes P$	$\mathcal{O}(v^2)$	$\cdots$	
$P \otimes S$	$\mathcal{O}(r_e^2 v^2)$	$\alpha_{\rm em}^2 v^2$	(2 loop)
$P \otimes P$	$\mathcal{O}(r_e^2 v^4)$	$\cdots$	
$V \otimes V$	1	1	(1 loop)
$V \otimes A$	$\mathcal{O}(v^2)$	$\cdots$	
$A \otimes V$	$\mathcal{O}(v^2)$	v^2	(1 loop)
$A \otimes A$	3	$\cdots$	
$T \otimes T$	12	q_ℓ^2	(1 loop)
$AT \otimes T$	$\mathcal{O}(v^2)$	$q_\ell^2 v^{-2}$	(1 loop)
	Scalar DM		
Γ_ℓ	$\sigma(\chi e \to \chi e)/\sigma^0_{\chi e,5}$	$\sigma(\chi N \to \chi N)/\sigma^1_{\chi N,5}$	
S	1	$\alpha_{\rm em}^2$	(2 loop)
P	$\mathcal{O}(v^2)$	$\cdots$	

B. Loop-induced DM-nucleus interactions

We have assumed that DM is leptophilic, so that at scale Λ only operators connecting DM to leptons, Eqs. (1), (2), and (4), are generated. However, even under this assumption, at loop level one does induce *model independently* also couplings to quarks from photon exchange between virtual leptons and the quarks. The diagrams that can arise at one- and two-loop order are shown in Fig. 2.[2] The lepton running in the loop can be either an electron or any other charged lepton to which the DM couples.

The one loop contribution involves the integral over loop momenta of the form

$$\int \frac{d^4q}{(4\pi)^4}\,\mathrm{Tr}\left[\Gamma_\ell \frac{\not{q}' + m_\ell}{q'^2 - m_\ell^2}\gamma^\mu \frac{\not{q} + m_\ell}{q^2 - m_\ell^2}\right], \tag{16}$$

with $q' = k - k' + q$ and k, k' the incoming momenta as denoted in Fig. 2 and Γ_ℓ the Dirac structures given in Eqs. (2) and (4). The one-loop contribution is nonzero only for vector and tensor lepton currents, $\Gamma_\ell = \gamma_\mu$, $\sigma_{\mu\nu}$. For the scalar lepton current, $\Gamma_\ell = 1$, the loop integral vanishes, reflecting the fact that one cannot couple a scalar current to a vector current. The DM-quark interaction is then induced at two loops through the diagrams shown in Fig. 2. In contrast for pseudoscalar and axial-vector lepton currents, $\Gamma_\ell = \gamma_5$, $\gamma_\mu\gamma_5$, the diagrams vanish to all loop orders. One insertion of γ_5 gives either zero or a fully antisymmetric tensor $\epsilon^{\alpha\beta\nu\mu}$. Since there are only three independent momenta in a $2 \to 2$ process, two indices need to be contracted with the same momentum, yielding zero.

The calculation of the one-loop and two-loop cross sections for scattering of DM on a nucleus is relegated to Appendix A. There we give the full one-loop expressions, whereas here we collect the main results in the "leading log" approximation, neglecting the remaining logarithmic dependence on momentum transfer. The approximate two-loop results are obtained in the limit of heavy leptons. Expanding also in the χ velocity $v \sim 10^{-3}$ to first nonzero order, the differential cross sections $d\sigma/dE_d$ are

$$\text{vector type:}\quad \frac{d\sigma}{dE_d} = \frac{d\sigma_N^1}{dE_d}\left[\log\left(\frac{m_\ell^2}{\mu^2}\right)\right]^2 \frac{1}{9}\left\{(c_V^\chi c_V^\ell)^2 + (c_A^\chi c_V^\ell)^2\left[v^2 + v_d^2\left(2 - \frac{m_N^2}{\mu_N^2}\right)\right]\right\} F(q)^2, \tag{17}$$

$$\text{tensor type:}\quad \frac{d\sigma}{dE_d} = \frac{d\sigma_N^1}{dE_d}\left[\log\left(\frac{m_\ell^2}{\mu^2}\right)\right]^2 \frac{4}{v_d^2}\frac{m_\ell^2}{m_N^2}\{c_T^2 v^2 + c_{AT}^2\} F(q)^2, \tag{18}$$

$$\text{scalar type:}\quad \frac{d\sigma}{dE_d} = \left(\frac{\alpha_{\mathrm{em}} Z}{\pi}\right)^2 \frac{d\sigma_N^1}{dE_d}\left(\frac{\pi^2}{12}\right)^2 \frac{m_N^2}{m_\ell^2} v_d^2 \left\{(c_S^\chi c_S^\ell)^2 + \frac{1}{4}(c_P^\chi c_S^\ell)^2 v_d^2 \frac{m_N^2}{m_\chi^2}\right\} \tilde{F}(q)^2, \tag{19}$$

$$\text{scalar DM:}\quad \frac{d\sigma}{dE_d} = \left(\frac{\alpha_{\mathrm{em}} Z}{\pi}\right)^2 \frac{d\sigma_{N,5}^1}{dE_d}\left(\frac{\pi^2}{12}\right)^2 \frac{m_N^2}{m_\ell^2} v_d^2 (d_S^\ell)^2 \tilde{F}(q), \tag{20}$$

where the common one-loop cross section prefactor is

$$\frac{d\sigma_N^1}{dE_d} = \frac{m_N}{2\pi v^2}\left(\frac{\alpha_{\mathrm{em}} Z}{\pi} G\right)^2, \tag{21}$$

and $d\sigma_{N,5}^1/dE_d$ is given by the same expression with $G \to G_5/(2m_\chi)$. Here m_N and Z are the nucleus mass and charge, respectively, while $\mu_N = m_N m_\chi/(m_N + m_\chi)$ is the reduced mass of the two-particle system. The two small parameters are the χ velocity $v \sim 10^{-3}$ and the velocity of the recoiled nucleus, $v_d = \sqrt{2E_d/m_N}$. The kinetic recoil energy of the nucleus E_d in the $\chi N \to \chi N$ scattering, cf. Equation (5), has a size $E_d \sim$ keV.

In the calculations we set $\mu = \Lambda$, since this is the scale at which the Wilson coefficient G is generated. The form factors $F(q)$ and $\tilde{F}(q)$ account for the nuclear structure. For the form factor $F(q)$ entering the one-loop induced scattering cross section we use [36] $F(q) = 3e^{-\kappa^2 s^2/2}[\sin(\kappa r) - \kappa r\cos(\kappa r)]/(\kappa r)^3$, with $s = 1$ fm, $r = \sqrt{R^2 - 5s^2}$, $R = 1.2A^{1/3}$ fm, $\kappa = \sqrt{2m_N E_d}$ (and $q^2 \simeq -\kappa^2$). The form factor $\tilde{F}(q)$ entering the two-loop expressions accounts for nuclear structure in the case of two-photon exchange. Its precise form is not needed in the subsequent analysis, though. The two-loop scalar-type differential cross section in Eq. (19) was calculated integrating out first the leptons assuming they are heavy. This is an appropriate limit for muon and tau intermediate states, where m_μ, $m_\tau \gg \kappa$, while for electrons $m_e \sim \kappa$ and the expression for the cross section is only approximate; see Appendix A for details.

For easier comparison with the previous section we also quote the results for the total $\chi N \to \chi N$ cross sections, integrated over the recoil energy E_d. For simplicity we neglect the dependence on the nuclear form factors and set $F(q) = \tilde{F}(q) = 1$ for this comparison, giving

[2]Similar diagrams with a photon replaced by a Z^0 or a Higgs boson are power suppressed by $(k - k')^2/M_{Z^0,H}^2$ and thus negligible.

$$\text{vector type: } \sigma = \sigma_N^1 \left[\log\left(\frac{m_\ell^2}{\mu^2}\right)\right]^2 \frac{1}{9}\left\{(c_V^\chi c_V^\ell)^2 + (c_A^\chi c_V^\ell)^2 v^2 \left[1 + \frac{1}{2}\frac{\mu_N^2}{m_N^2}\right]\right\}, \tag{22}$$

$$\text{tensor type: } \sigma = \sigma_N^1 \left[\log\left(\frac{m_\ell^2}{\mu^2}\right)\right]^2 \frac{m_\ell^2}{\mu_N^2}\left\{c_T^2 + c_{AT}^2 \frac{1}{v^2}\right\} \log\left(\frac{E_d^{\max}}{E_d^{\min}}\right), \tag{23}$$

$$\text{scalar type: } \sigma = \left(\frac{\alpha_{\rm em} Z}{\pi}\right)^2 \sigma_N^1 \left(\frac{\pi^2}{12}\right)^2 \left(\frac{\mu_N v}{m_\ell}\right)^2 \left\{2(c_S^\chi c_S^\ell)^2 + \frac{4}{3}(c_P^\chi c_S^\ell)^2 v^2 \frac{\mu_N^2}{m_\chi^2}\right\}, \tag{24}$$

$$\text{scalar DM: } \sigma = \left(\frac{\alpha_{\rm em} Z}{\pi}\right)^2 \sigma_{N,5}^1 \left(\frac{\pi^2}{12}\right)^2 \left(\frac{\mu_N v}{m_\ell}\right)^2 2(d_S^\ell)^2, \tag{25}$$

where σ_N^1 is the integral of the differential cross section of Eq. (21)

$$\sigma_N^1 = \frac{\mu_N^2}{\pi}\left(\frac{\alpha_{\rm em} Z}{\pi} G\right)^2 \approx 1.9 \times 10^{-32}\ \text{cm}^2 \left(\frac{\Lambda}{10\ \text{GeV}}\right)^{-4} \left(\frac{\mu_N}{10\ \text{GeV}}\right)^2 \left(\frac{Z}{53}\right)^2, \tag{26}$$

and $\sigma_{N,5}^1$ is obtained from the above expression with $G \to G_5/(2m_\chi)$. The above results are summarized in Table I, facilitating comparison with χ scattering on free electrons. In Table I we took $\mu_N \sim m_N \sim m_\chi$, while the scaling for other values of nucleon and DM masses is easy to obtain from the above results.

C. Discussion of Lorentz structures

In Sec. II B we have estimated a strong hierarchy between the three types of signals as $R^{\rm WAS} \ll R^{\rm WES} \ll R^{\rm WNS}$; see Eq. (9). These results imply that whenever WNS at one loop or two loop is generated it dominates the event rate in direct detection experiments. The Lorentz structures for which this situation applies can be read off from Table I. To be specific we will use as a representative example of this class the $V \otimes V$ coupling in the rest of this paper. From the table we also see that there is one case—the $A \otimes A$ coupling—where no χN scattering is induced at loop level and moreover the WIMP-electron cross section is not additionally v and/or m_e/m_χ suppressed. Hence, we chose the $A \otimes A$ coupling as our second representative example to quantitatively discuss the case of a WES dominated event rate. The results from these two examples can be qualitatively extrapolated to other Lorentz structures using Table I.

As we will see in the following, the $\chi e \to \chi e$ cross section in the $A \otimes A$ case has to be very large [corresponding to $\Lambda \sim \mathcal{O}(100\ \text{MeV})$] in order to be relevant for DAMA. For the cases in Table I where $\sigma_{\chi e}^0$ is further suppressed by small numbers, like for example $S \otimes P$ or $P \otimes P$, the scale Λ would have to be even lower, so that the effective field theory description would break down.

Finally, let us mention the tensor coupling $T \otimes T$, where the one-loop cross section is suppressed by m_ℓ^2/m_N^2, while χe scattering is enhanced by a factor of 12. If DM couples *only* to the electron and not to μ and τ the suppression of the loop is of order $m_e^2/m_N^2 \sim 10^{-10}$, and hence, WES and WNS rates can be of comparable size. However, in general one expects also a coupling to the μ and τ leptons. To be specific, in our numerical analysis of $V \otimes V$ and $A \otimes A$ cases we will assume equal couplings to all three leptons. For the tensor case the same choice would mean that WNS dominates.

IV. EVENT RATES

In this section we provide the event rates in direct detection experiments. For WES and WAS we assume $A \otimes A$ coupling and for WNS we take $V \otimes V$. These rates will be used for the numerical fits to DAMA, CDMS, and XENON data in the following. As argued above, the $A \otimes A$ and $V \otimes V$ cases are representative enough to cover qualitatively all possible Lorentz structures.

The differential counting rate in a direct DM detection experiment (in units of counts per energy per kg detector mass per day) is given by

$$\frac{dR}{dE_d} = \frac{\rho_0}{m_\chi}\frac{\eta}{\rho_{\rm det}} \int d^3v\, v \frac{d\sigma}{dE_d} v f_\odot(\mathbf{v}), \tag{27}$$

where $E_d = E_\chi - E_\chi'$ is the energy deposited in the detector, ρ_0 is the local DM density (which we take to be $0.3\ \text{GeV}\,\text{cm}^{-3}$), η is the number density of target particles, and $\rho_{\rm det}$ is the mass density of the detector. If the target contains different elements (like in the case of the DAMA NaI crystals), the sum over the corresponding counting rates is implied.

In Eq. (27), $f_\odot(\mathbf{v})$ is the local WIMP velocity distribution in the rest frame of the detector, normalized according to $\int d^3v f_\odot(\mathbf{v}) = 1$. It follows from the DM velocity distribution in the rest frame of the galaxy, $f_{\rm gal}(\mathbf{v})$, by a Galilean transformation with the velocity of the Sun in the Galaxy and the motion of the Earth around the Sun. For $f_{\rm gal}(\mathbf{v}) = f_{\rm gal}(v)$ we assume the conventional Maxwellian

distribution with $\bar{v} = 220$ kms^{-1} and a cutoff due to the escape velocity from the galaxy of $v_{\rm esc} = 650$ kms^{-1}: $f_{\rm gal}(v) \propto \exp(-v^2/\bar{v}^2) - \exp(v_{\rm esc}^2/\bar{v}^2)$ for $v \leq v_{\rm esc}$ and zero for $v > v_{\rm esc}$. We have checked that the precise value of the escape velocity has a negligible impact on our results.

A scattered nucleus does not deposit all its energy in the form of scintillation light. This effect is taken into account by the so-called quenching factors, which are $q_{\rm Na} \simeq 0.3$ for sodium recoils and $q_{\rm I} \simeq 0.085$ for iodine recoils [37] in DAMA. In Refs. [38,39] it has been pointed out that the so-called channeling effect could be relevant, implying that for a certain fraction of events no quenching would occur due to the special orientation of the recoil with respect to the crystal. So far this effect has not been confirmed experimentally in the relevant energy range. Indeed, the results of Ref. [40] do not indicate the presence of any variation of the count rate for special crystal directions. Quenching and channeling is relevant in DAMA in the cases of WAS and WNS, while the scattered electrons in the case of WES produce unquenched scintillation light. In our fit to DAMA data for WNS we do include channeling following Ref. [39] (similar as in [10]), but we comment also on the case when no channeling occurs.

A. WIMP-electron scattering

To obtain an expression for the event rate in the case of WES it is necessary to take into account the fact that electrons are bound to the atoms. The kinematics of scattering off bound electrons has some important differences compared to scattering off free particles. The bound electron does not obey the free-particle dispersion relation $E_{e({\rm free})}^2 = p^2 + m^2$. Instead it has a fixed energy $E_e = m_e - E_B$, determined by the binding energy of the atomic shell, $E_B \geq 0$, whereas its momentum p follows a distribution which is given by the square of the Fourier transform of the bound state wave function corresponding to that shell. Energy conservation reads in this case $E_\chi + m_e - E_B = E'_\chi + E'_e$, or

$$E'_e = m_e + E_d - E_B. \tag{28}$$

After some tedious algebra one arrives at the following expression for E_d:

$$E_d \approx -\frac{p^2}{2m_\chi} - pv\cos\theta, \tag{29}$$

where[3] $\cos\theta = \mathbf{kp}/kp$ and we used the approximation $E_d \ll m_e \leq E_e \ll m_\chi$ and $v \sim 10^{-3}$. We see that to obtain detectable energies relevant for DAMA (E_d of a few keV), electron momenta of order MeV are required.

[3]We always denote the DM momentum with $\mathbf{k}$ and the electron (or nucleus) momentum with $\mathbf{p}$, see Fig. 1. Bold symbols refer to 3-vectors and $k \equiv |\mathbf{k}|$, and similar for p.

In Appendix B we give the details on the calculation of the scattering cross section and count rate in the case of WES, taking into account the peculiarities of scattering on bound electrons. Here we only report the final results. Assuming the axial-vector Dirac structure, $\Gamma_\chi = \Gamma_e = A$, as motivated above, the count rate is (we also set $c_A^\chi = c_A^e = 1$ for simplicity)

$$\frac{dR^{\rm WES}}{dE_d} \simeq \frac{3\rho_0 m_e G^2}{4\pi(m_{\rm I} + m_{\rm Na})m_\chi} \sum_{nl} \sqrt{2m_e(E_d - E_{B,nl})}(2l+1) \times \int \frac{dpp}{(2\pi)^3} |\chi_{nl}(p)|^2 I(v_{\rm min}^{\rm WES}). \tag{30}$$

Here $\chi_{nl}(p)$ is the momentum wave function of the electron, and the function $I(v_{\rm min})$ is

$$I(v_{\rm min}) \equiv \int d^3v \frac{f_\odot(\mathbf{v})}{v} \theta(v - v_{\rm min}), \tag{31}$$

while the minimal velocity required to give detectable energy E_d follows from Eq. (29):

$$v_{\rm min}^{\rm WES} \approx \frac{E_d}{p} + \frac{p}{2m_\chi}. \tag{32}$$

For $m_\chi \gtrsim 10$ GeV and p of order MeV the first term dominates.

The sum in Eq. (30) is over the atomic shells of both iodine and sodium with quantum numbers nl, and $E_{B,nl}$ is the corresponding binding energy. The electron can only be kicked out of its atomic shell if its binding energy is smaller than the total energy deposited in the detector [cf. Eq. (28)]:

$$E_d \geq E_{B,nl}. \tag{33}$$

Only the shells satisfying this requirement can contribute to the event rate in Eq. (30). The momentum wave function $\chi_{nl}(p)$ is defined in Eq. (B3) in Appendix B. Technical details on how we implement the wave function numerically are given in Appendix C; the results for the iodine and sodium wave functions are shown in Fig. 3. We see that the dominant contribution to WES scattering in DAMA comes from the inner s shells of iodine because these are largest at high p. Electrons from the $1s$, $2s$, $2p$ shells—depicted as thin light curves in Fig. 3—do not contribute to the DAMA signal region of $E_d \simeq 2$–4 keV since the binding energies are too large, respectively, 33.2, 5.2, and 4.7 keV [41]. The shell dominating the signal in the 2–4 keV region is the $3s$ shell of iodine, with a binding energy of about 1 keV. Apparently this has been overlooked in Ref. [28], while it has important consequences on the size of the needed cross section; see the discussion in Sec. V B.

B. WIMP-atom scattering

Let us consider now the case when the electron on which the DM particle scatters remains bound and the recoil is taken up by the whole atom. According to the coordinate

space Feynman rules, the matrix element for WAS for an electron in atomic shell nlm in the initial state and $n'l'm'$ in the final state is given by

$$\mathcal{M}^{rr's s'}_{nlm,n'l'm'} = G \int d^3x \psi^*_{n'l'm'}(\mathbf{x}) \psi_{nlm}(\mathbf{x}) e^{-i\mathbf{p}'\mathbf{x}} e^{i(\mathbf{k}-\mathbf{k}')\mathbf{x}} \times \bar{u}^{r'}_{\chi} \Gamma^{\mu}_{\chi} u^{r}_{\chi} \bar{u}^{s'}_{e} \Gamma_{e\mu} u^{s}_{e}. \tag{34}$$

Here, $\mathbf{k}$ and $\mathbf{k}'$ are the initial and final momenta of the WIMP, and $\mathbf{p}'$ is the average momentum of the electron in the final state resulting from the motion of the whole atom after the scattering. Since most of the recoil momentum is carried by the nucleus, $|\mathbf{p}'|$ is smaller than $|\mathbf{k}-\mathbf{k}'|$ by a factor of m_e/m_N, and can therefore be neglected. The coordinate space wave function of the electron in the state with orbital quantum numbers nlm is denoted by $\psi_{nlm}(\mathbf{x})$. Again we specialize to the case of axial-vector coupling, $\Gamma^{\mu}_{\chi} = \Gamma^{\mu}_{e} = \gamma^{\mu}\gamma^5$ and set $c^{\chi}_{A} = c^{e}_{A} = 1$. We use nonrelativistic spinors, which is certainly justified for u^{r}_{χ} and $u^{r'}_{\chi}$, and also for u^{s}_{e} except, perhaps, for electrons from the $1s$ shell of iodine. In this last case, relativistic corrections are of order 20%.

Let us first consider the case when the electron remains in its state, and hence the scattering on the atom is elastic (el-WAS). Then we have $s = s'$ and $nlm = n'l'm'$. Furthermore, we have to sum coherently over all shells and electron spins, since it is impossible in principle to identify on which electron the WIMP has scattered. It turns out that for the axial-vector case the spin sum $\sum_s \bar{u}^{s}_{e}\gamma^{\mu}\gamma^5 u^{s}_{e}$ vanishes. This can be verified by using explicit expressions for the spinors u^{s}_{e}, and follows from the fact that the different sign due to γ_5 of right-handed and left-handed components of the electron cancel each other in the case of a coherent sum over spins.[4] The elastic scattering may be relevant for other Lorentz structures where this cancellation does not occur. However, in Sec. III C we have argued that the only case of practical relevance is the axial coupling, and therefore we will not consider el-WAS further.

We are left now with the case where the electron is excited to an outer free shell which corresponds to inelastic WIMP-atom scattering (ie-WAS). In this case the sum over all occupied electron states nlm, over all unoccupied states $n'l'm'$, and over WIMP and electron spins has to be incoherent because one can distinguish in principle different initial and final states, e.g. by x-ray spectroscopy. The differential cross section in this case is obtained as

$$\frac{d\sigma^{\mathrm{WAS}}}{dE_d} = \frac{m_N \overline{|\mathcal{M}|^2}}{32\pi m_e^2 m_\chi^2 v^2}. \tag{35}$$

[4]This argument will not hold if an unpaired valence electron is available so that we cannot sum over spins. However, most chemically bound systems are formed in such a way that this does not happen. Even in this case el-WAS would be suppressed since scattering on outer electrons is highly suppressed by the smallness of the binding energy of these electrons compared to the transferred momentum.

Plugging in the matrix element from Eq. (34) we get

$$\frac{d\sigma^{\text{ie-WAS}}}{dE_d} = \frac{3m_N G^2}{2\pi v^2} \sum_{nlm} \sum_{n'l'm'} |\langle n'l'm'|e^{i(\mathbf{k}-\mathbf{k}')\mathbf{x}}|nlm\rangle|^2, \tag{36}$$

with

$$\langle n'l'm'|e^{i(\mathbf{k}-\mathbf{k}')\mathbf{x}}|nlm\rangle \equiv \int d^3x \psi^*_{n'l'm'}(\mathbf{x}) \psi_{nlm}(\mathbf{x}) e^{i(\mathbf{k}-\mathbf{k}')\mathbf{x}}. \tag{37}$$

The expression for the counting rate is obtained from Eq. (27),

$$\frac{dR^{\text{ie-WAS}}_N}{dE_d} = \frac{m_N}{m_{\mathrm{I}} + m_{\mathrm{Na}}} \frac{3\rho_0 G^2}{2\pi m_\chi} \times \sum_{nlm} \sum_{n'l'm'} |\langle n'l'm'|e^{i(\mathbf{k}-\mathbf{k}')\mathbf{x}}|nlm\rangle|^2 I(v^{\text{ie-WAS}}_{\min}), \tag{38}$$

with $N = \mathrm{I}, \mathrm{Na}$. The function I is defined in Eq. (31), and the minimal velocity required to give detectable energy E_d follows from the kinematics implied by energy conservation, $E_d = E_\chi - E'_\chi = \delta E_B + m_N v_N^2/2$, and momentum conservation, $\mathbf{k} = \mathbf{k}' + m_N \mathbf{v}_N$:

$$v^{\text{ie-WAS}}_{\min} = \frac{E_d(m_\chi + m_N) - m_N \delta E_B}{m_\chi \sqrt{2m_N(E_d - \delta E_B)}}, \tag{39}$$

where δE_B is the difference of the binding energies of the initial and final shells: $\delta E_B = E_{B,nlm} - E_{B,n'l'm'}$. Details on how we calculate the matrix elements involving the wave function in Eq. (38) are given in Appendix C.

C. Loop-induced WIMP-nucleus scattering

The event rate for loop-induced DM-nucleus scattering is easy to obtain from the differential cross sections $d\sigma_N/dE_d$ in Eqs. (17)–(20) and the general expression for the counting rate Eq. (27):

$$\frac{dR^{\mathrm{WNS}}_N}{dE_d} = \frac{\rho_0}{m_\chi} \frac{1}{m_{\mathrm{I}} + m_{\mathrm{Na}}} \left(\frac{d\sigma_N}{dE_d} v^2\right) I(v^{\mathrm{WNS}}_{\min}). \tag{40}$$

The function I is defined in Eq. (31), while the minimal velocity to produce a detectable energy E_d is given for WIMP-nucleus elastic scattering by $v^{\mathrm{WNS}}_{\min} = \sqrt{E_d m_N/2\mu_N^2}$ with $\mu_N = m_\chi m_N/(m_\chi + m_N)$.

We now specialize to the $V \otimes V$ case. The event rate depends on the χ mass and the coupling constant of the effective operator G (we set $c^{\chi}_{V} = c^{\ell}_{V} = 1$ from now on). For easier comparison with previous works, it is useful to trade G for the total $\chi e \to \chi e$ cross section $\sigma^0_{\chi e} = G^2 m_e^2/\pi$, Eq. (13). For the $V \otimes V$ case we thus have

$$\frac{d\sigma_N}{dE_d} v^2 = \sigma^0_{\chi e} \times \frac{m_N}{18 m_e^2} \left(\frac{\alpha Z}{\pi}\right)^2 F(q)^2 \left[\log\left(\frac{m_\ell^2}{\mu^2}\right)\right]^2, \quad (41)$$

to be inserted in Eq. (40). As discussed in Appendix A this leading log approximation is quite accurate. Nevertheless, in the numerical calculations we use the full expressions given in Appendix A. We set $\mu = 10$ GeV, since this corresponds roughly to the scale Λ, where our effective theory is defined. Furthermore, we assume (somewhat arbitrarily) equal couplings to all three leptons. The logarithm in Eq. (41) implies then a relative contribution of $e{:}\mu{:}\tau \simeq 30{:}7{:}1$. Note that the rate is dominated by the contribution from the electron in the loop assuming equal couplings at the scale $\Lambda \sim 10$ GeV. Therefore, our results are conservative, in the sense that per assumption DM has to couple to the electron.

V. FIT RESULTS FOR DAMA, CDMS, AND XENON10

A. Vectorlike interactions and loop-induced WIMP-nucleon scattering

The event rate in the case of the loop-induced WNS, Eq. (40), is very similar to the corresponding expression for usual spin-independent elastic WIMP scattering on the nucleus (see, e.g., Refs. [10,11,36]), denoted as the "standard case" in the following. The main difference is the replacement of the atomic mass number A by the charge number Z (and an additional logarithmic E_d dependence beyond the leading log approximation). Therefore we expect that the fit of DAMA and the compatibility to CDMS and XENON will be very similar to the standard case, see e.g., Refs. [9–11].

Our numerical analysis of DAMA, CDMS, and XENON data closely follows Ref. [10] where technical details on the fit can be found. For the DAMA fit we use the spectral data on the annual modulation amplitude S_m from the threshold of 2 keV up to 8 keV. The data above this energy are consistent with no modulation and since our model does not predict any features in that region they do not provide an additional constraint on the fit, apart from diluting the overall goodness of fit. In addition to the data on the amplitude of the modulated count rate we use also the unmodulated event rate as a constraint in the fit. While the bulk of these events will come from various unidentified backgrounds, every model has to fulfill the constraint of not predicting more unmodulated events than actually observed in DAMA. Figure 4 shows the predicted spectrum at the best fit point compared to the DAMA data. Note that the error bars on the unmodulated rate (lower panel) are hardly visible for most of the data points, as a result of the huge number of events in DAMA. For the analysis using data from 2–8 keV the best fit point is at $m_\chi = 12.4$ GeV, $\sigma^0_{\chi e} = 4.5 \times 10^{-44}$ cm^2, and we obtain the excellent fit of $\chi^2/\mathrm{dof} = 9.1/10$. If we drop the first data point the fit even improves to $\chi^2/\mathrm{dof} = 2.8/9$.

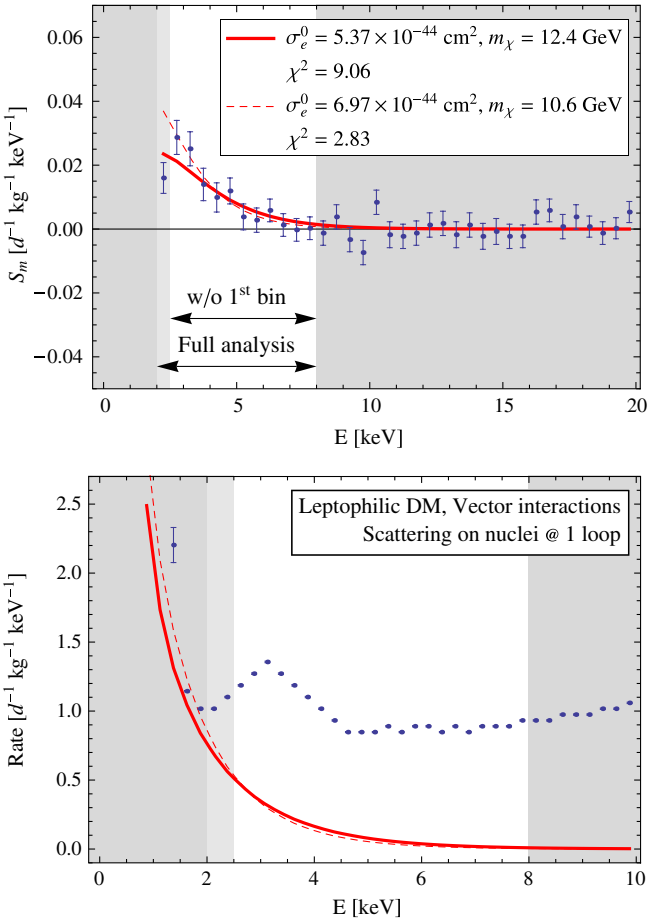

FIG. 4 (color online). Predicted spectrum for the modulated (top panel) and unmodulated (bottom panel) event rate in DAMA at the best fit point assuming loop-induced WIMP-nucleus scattering resulting from vectorlike DM-lepton couplings. Results are shown for using all data points from 2–8 keV (solid lines) and for omitting the 1st bin (dashed lines). The parameter values and the χ^2 values are given in the legend.

The allowed regions in the plane of DM mass and scattering cross section are shown in Fig. 5. For easier comparison with the case of scattering off electrons we parametrize the cross section on the vertical axis in terms of $\sigma^0_{\chi e}$; see Eq. (41). The spectral data on the modulated signal results in an allowed region for rather small DM masses around $m_\chi \simeq 12$ GeV. If channeling is not taken into account an allowed region appears at similar DM masses but at higher cross sections (due to scattering off sodium [42]).[5] This DAMA allowed region has to be compared to the constraints from CDMS and XENON. The compatibility with these bounds is similar to the

[5]In both cases (with and without channeling) there is also a local minimum around a WIMP mass of about 80 GeV from unchanneled scatterings off iodine. In Fig. 5 we show confidence regions defined with respect to the global minimum, and this second region does not appear at 3σ if channeling is included.

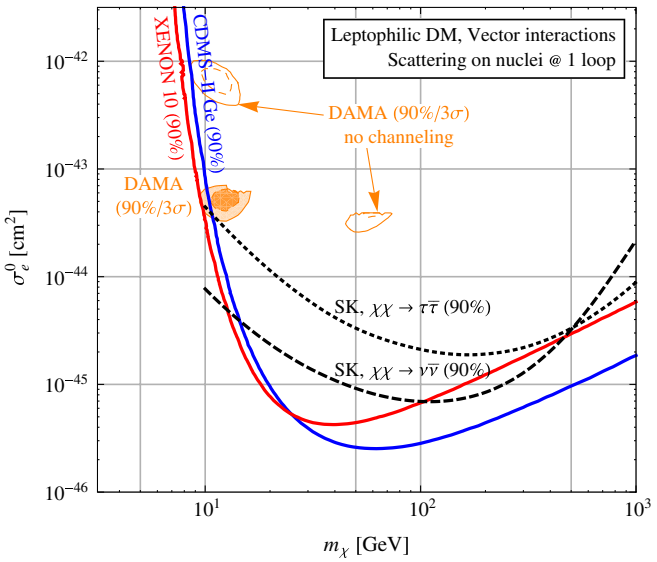

FIG. 5 (color online). DAMA allowed region at 90% and 3σ C.L. in the case of one-loop induced WIMP-nucleus scattering ($V \otimes V$ coupling) in the plane of the WIMP mass and the WIMP-electron cross section $\sigma^0_{\chi e} = G^2 m_e^2/\pi$. Regions are shown with and without taking into account the channeling effect. Furthermore, we show the bounds at 90% C.L. from CDMS-II and XENON10. The dashed curves show the 90% C.L. constraint from the Super-Kamiokande limit on neutrinos from the Sun, by assuming annihilation into $\tau\bar{\tau}$ or $\nu\bar{\nu}$; see Sec. VI for details.

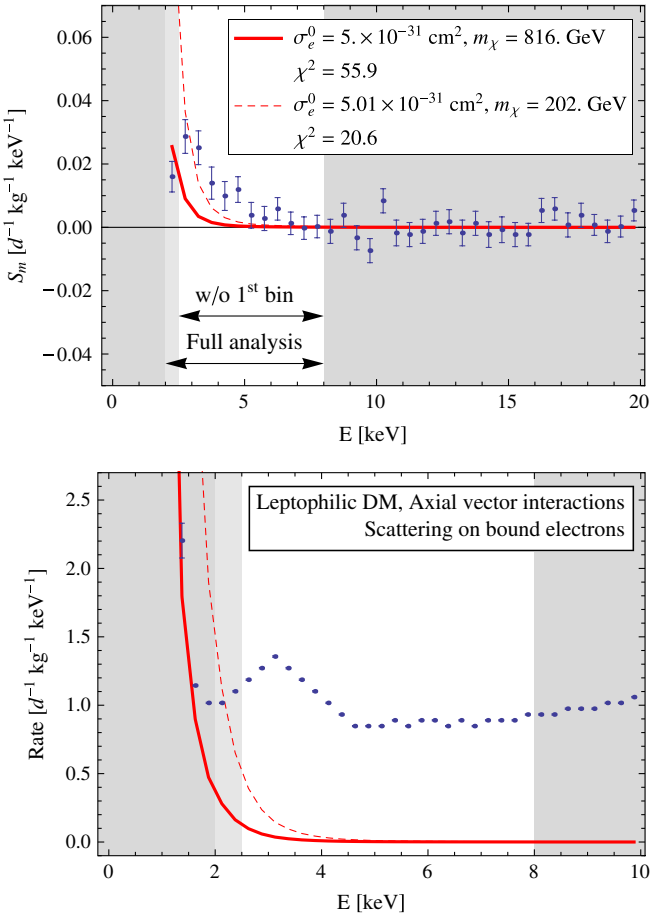

FIG. 6 (color online). Predicted spectrum for the modulated (top panel) and unmodulated (bottom panel) event rate in DAMA at the best fit point assuming WIMP-electron scattering resulting from axial-vectorlike DM-electron couplings. Results are shown for using all data points from 2–8 keV (solid lines) and for omitting the 1st bin (dashed lines). The parameter values and the χ^2 values are given in the legend.

standard case: while marginal compatibility might remain there is clearly severe tension between the DAMA signal and the CDMS and XENON bounds in this framework. Here we will not elaborate on this question further and refer to Refs. [9–11] for detailed discussions of the DAMA versus CDMS/XENON compatibility in the standard case.

The main motivation for considering electron interacting DM—namely, avoiding the constraints from nuclear recoil experiments, is thus invalidated by the loop-induced nucleon scattering. We now turn to the axial-axial coupling, where the loop-induced scattering can be avoided.

B. Axial-vectorlike interactions and WIMP-electron scattering

We perform a similar fit to DAMA data as before but using now Eq. (30) for the event rate for WES. The predicted modulated and unmodulated DAMA event rates at the best fit in this case are shown in Fig. 6. Using the data from 2–8 keV we obtain a rather bad fit to the modulated spectrum with $\chi^2/\text{dof} = 55.9/10$, which corresponds to a probability of 2×10^{-8}. The prediction drops too fast with energy in order to provide a satisfactory fit to the data. If we omit the first energy bin the fit improves considerably to $\chi^2/\text{dof} = 20.6/9$ corresponding to a probability of 1.4%. We find, however, that the parameter values from this fit predict a very sharp rise for the spectrum of the unmodulated event rate in DAMA, see the lower panel of Fig. 6. In the fit we have required that the unmodulated prediction stays below the observed rate within the analysis window down to 2 keV. However, DAMA shows also some data points for the unmodulated rate below 2 keV, which are not compatible with the predicted rate. While it is not possible to use data below 2 keV for the modulation, it seems likely that they rule out models predicting more events than observed. The WES fit shown as a dashed curve in Fig. 6 predicts more than a factor of 3 more events than observed in the first two bins below 2 keV, where error bars are still very small. We conclude that WES has severe problems to explain the spectral shapes of the modulated and unmodulated components of DAMA data.

If we ignore the problems of the spectral fit and despite the low goodness of fit consider "allowed regions" in the plane of WIMP mass and cross section relative to the best fit point we obtain the results shown in Fig. 7. We observe

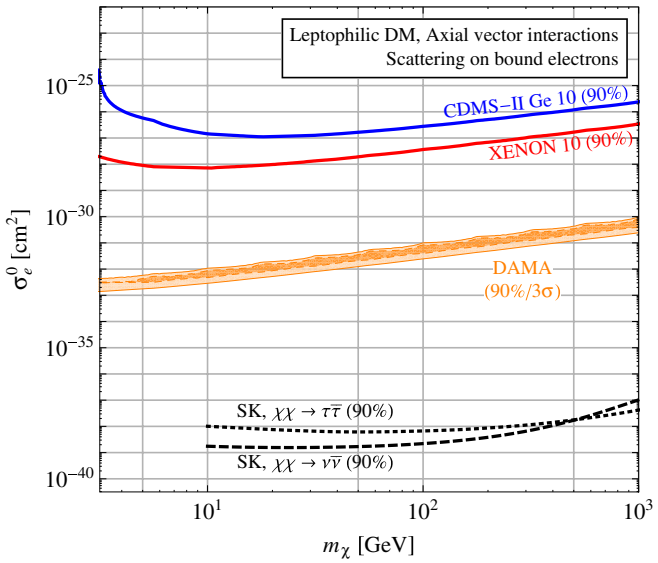

FIG. 7 (color online). DAMA allowed region at 90% and 3σ C.L. in the case of WIMP-electron scattering (axial-axial coupling) in the plane of the WIMP mass and the WIMP-electron cross section $\sigma^0_{\chi e} = G^2 m_e^2/\pi$. We stress that these regions are obtained with respect to the best fit point, which by itself does not provide a satisfactory fit to DAMA modulated and unmodulated spectral data; see Fig. 6. We show also the bounds at 90% C.L. from CDMS-II and XENON10 from inelastic WIMP-atom scattering. The dashed curves show the 90% C.L. constraint from the Super-Kamiokande limit on neutrinos from the Sun, by assuming annihilation into $\tau\bar{\tau}$ or $\nu\bar{\nu}$; see Sec. VI for details.

that very large cross sections are required:

$$\sigma^0_{\chi e} \sim 10^{-31}\ \mathrm{cm}^2 \times \left(\frac{m_\chi}{100\ \mathrm{GeV}}\right), \tag{42}$$

where the linear dependence on m_χ holds for $m_\chi \gtrsim 10$ GeV. The vastly different best fit cross sections for WNS and WES follow from the discussion in Sec. II B where we estimated the relative size of the corresponding counting rates; see Eq. (9). Here we do not explore other phenomenological consequences of such a large cross section. Just note from Eq. (13) that we can realize a cross section of this order of magnitude only with a relatively low scale for the new physics of $\Lambda \lesssim 0.1$ GeV, where we have assumed for the couplings $c_A^\chi \sim c_A^e \sim 1$. If in a particular model constraints on the coupling constant c_A^e apply (see, for example [43]), Λ has to be accordingly smaller. Note that the momentum transfer for WES is given by the momentum of the bound electron, which has to be of order MeV. This provides a lower bound on Λ in order to describe the interaction by using the effective theory.

The cross section from Eq. (42) is about 5 orders of magnitude larger than the result obtained in Ref. [28], which finds pb-size $\sigma^0_{\chi e}$ at $m_\chi \sim 100$ GeV. Let us comment, therefore, on the differences of our analysis to the one from [28]. Apparently the main difference is that we take into account the special kinematics related to the scattering off bound electrons, whereas in Ref. [28] electrons are treated as effectively free with a momentum distribution obtained from the wave function. Our calculation outlined in Sec. IV A and Appendix B leads to several suppression factors in the WES event rate with respect to the expression used in [28]. Our minimal velocity $v_{\mathrm{min}}^{\mathrm{WES}}$ from Eq. (32) is roughly a factor of 2 larger than the one used in [28] requiring one to go farther out in the tail of the WIMP velocity distribution. Furthermore, the condition Eq. (33), $E_d \geq E_B$, which prevents the contribution of the inner shells of iodine, has not been imposed in [28]. From Fig. 3 we see that at $p \sim 1$ MeV the wave function of the iodine $1s$ shell is about 2 orders of magnitude larger than the one of the $3s$ shell, which actually gives the first relevant contribution after requiring that the binding energy be lower than $E_d \sim$ few keV.

As mentioned above, in the case under consideration inelastic WAS may contribute to experiments searching for nuclear recoils. To calculate this effect we would have to perform the sum in Eq. (38) over all occupied shells nlm and all free shells $n'l'm'$. It turns out numerically that transitions from s shells to s shells give the largest contributions; see also Appendix C. In order to estimate the order of magnitude we have taken into account transitions from the $1s$, $2s$, and $3s$ orbitals to the first two free s orbitals of the germanium and xenon nuclei relevant in CDMS and XENON, respectively. In Fig. 7 we show the constraints resulting from this estimate of the ie-WAS event rate. Numerically these constraints turn out to be very weak and the limits are several orders of magnitude above the region indicated by DAMA; the good sensitivities of CDMS and XENON to nuclear recoils cannot compensate the large suppression of the ie-WAS count rate compared to WES, as estimated in Eq. (9).

Although the poor quality of the fit in the case of WES already disfavors this mechanism as an explanation for the DAMA modulation signal, we will show in the next section that constraints on neutrinos from DM annihilations inside the Sun are even more stringent and exclude the cross sections required for DAMA by many orders of magnitude if DM annihilations provide neutrinos in the final states.

VI. NEUTRINOS FROM DM ANNIHILATIONS INSIDE THE SUN

Any DM candidate has to fulfill the constraints on the upward through-going muons coming from water Cerenkov detectors, like Super-Kamiokande [16], and from neutrino telescopes [44–46]. Some recent papers [17,47] have discussed the constraints on the DAMA region in the framework of standard WIMP-nucleus scattering. Here, we reanalyze the bound coming from the Super-Kamiokande experiment in the framework of leptonically interacting DM.

One important ingredient for the prediction of the neutrino flux coming from DM annihilations inside a celestial

body is the capture rate $C_\odot$, which is proportional to the DM scattering cross section; see, e.g. [36]. In the calculation of this quantity, usually, the WIMPs are assumed to interact with material at zero temperature, neglecting the solar temperature of about 1.5×10^7 K in the center and 8.1×10^4 K at the surface. Although this is a reasonable assumption for WIMP candidates interacting with hydrogen and the other nuclei inside the Sun, it fails for the case of DM scattering on the free electrons in the Sun. The effect of nonzero temperature on the capture rate depends on the ratio of the thermal velocity of the target to the WIMP velocity. The thermal kinetic energy $k_B T$ is independent of the mass, but the thermal velocity is larger by a factor $\sqrt{m_p/m_e} \simeq 45$ for electrons compared to hydrogen.

We calculate the rate for WIMP capture by a body at finite temperature following Ref. [48], where the expression given there has to be extended to include the motion of the Sun with respect to the DM halo. The temperature distribution for the electrons inside the Sun is taken from the solar model BS2005-AGS, OP [49]. Figure 8 shows the effect of the nonzero temperature on the capture rate for electrons, hydrogen, and all other nuclei in the Sun. We find that the capture rate on electrons is enhanced by about 1 order of magnitude, while the effect is hardly visible at the scale of the plot for hydrogen. The temperature effect can be neglected for scattering off heavier nuclei, which dominates the capture in the case of loop-induced WNS. In this case one has to include also a suppression due to the nuclear form factor. Furthermore, we neglect the effect of WIMP evaporation, important only for DM masses lower than 10 GeV [50] and the gravitational effects from planets like Jupiter [51].

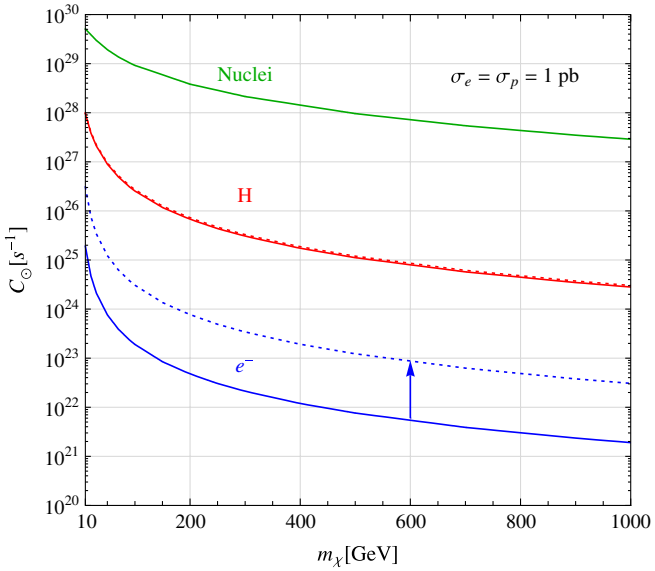

FIG. 8 (color online). WIMP capture rate in the Sun as a function of the WIMP mass assuming DM scattering off electrons, hydrogen, and all other nuclei in the Sun, with a scattering cross section of 10^{-36} cm^2. The solid curves correspond to scattering off particles at zero temperature, whereas the dotted curves show the effect of the actual temperature distribution inside the Sun [49] for electrons and hydrogen.

The annihilation rate $\Gamma_\odot$ is related to the capture rate $C_\odot$ by [36]

$$\Gamma_\odot = \frac{C_\odot}{2} \tanh^2\left(\frac{t_\odot}{\tau}\right), \qquad \tau = \frac{1}{\sqrt{C_\odot C_A}}, \tag{43}$$

where $t_\odot \simeq 4.5$ Gyr is the age of the Sun and the parameter C_A depends on the WIMP annihilation cross section and on the effective volume of the confining region in which the DM particles are trapped: $C_A = \langle \sigma_{\rm ann} v \rangle V_2 / V_1^2$ with $V_j = 6.6 \times 10^{28} (j m_\chi / 10\ {\rm GeV})^{-3/2}$ cm^3. We denote by $\langle \sigma_{\rm ann} v \rangle$ the thermally averaged total annihilation cross section times the relative velocity, at the present time. Capture and annihilation are in equilibrium if $\tau \ll t_\odot$. Then the annihilation rate is just half the capture rate and becomes independent of the annihilation cross section $\langle \sigma_{\rm ann} v \rangle$. For our calculations we assume this limit; we comment on its validity in Appendix D.

The neutrino flux at the detector from the annihilation channel f with branching ratio BR_f is given by

$$\frac{d\phi_\nu^f}{dE_\nu} = \mathrm{BR}_f \frac{\Gamma_\odot}{4\pi d^2} \frac{dN_\nu^f}{dE_\nu}, \tag{44}$$

with d being the distance between the Earth and the Sun. Here we are interested in annihilations into leptons. We consider the following four channels: $\tau\bar{\tau}$, $\nu_e \bar{\nu}_e$, $\nu_\mu \bar{\nu}_\mu$, and $\nu_\tau \bar{\nu}_\tau$. Note that annihilations into electrons do not provide neutrinos, and muons are always stopped before decay, giving rise to neutrinos in the MeV energy range which is below the Super-Kamiokande threshold [52]. In the case of direct neutrino channels, the initial neutrino spectrum is simply a Dirac δ function centered at $E_\nu = m_\chi$, and we assume a flavor-blind branching ratio, i.e., $\mathrm{BR}_{\nu_e\bar{\nu}_e} = \mathrm{BR}_{\nu_\mu\bar{\nu}_\mu} = \mathrm{BR}_{\nu_\tau\bar{\nu}_\tau} = 1/3$. The results do not depend strongly on this assumption, since flavors are mixed due to oscillations.[6] For the $\tau\bar{\tau}$ channel, we use the initial neutrino spectrum given in [53].

The neutrino spectrum dN_ν^f/dE_ν at the detector is calculated considering the effect of neutrino oscillation, coherent Mikheyev-Smirnov-Wolfenstein matter effect, absorption, and regeneration (see e.g., [53,54]) by solving numerically the evolution equations of the neutrino density matrix within the Sun. The neutrino oscillation parameters

[6]There is some difference of the $\nu_\tau\bar{\nu}_\tau$ channel due to τ regeneration effects, which are important for high energies. Assuming annihilations with branching ratios equal to one for each of the three flavors we find that the muon neutrino flux at the Earth is practically the same for all three initial flavors up to $m_\chi \simeq 100$ GeV. For $m_\chi = 1$ TeV the ratio of the muon neutrino fluxes at Earth is roughly 1:3.5:6.4 for annihilations into $\nu_e\bar{\nu}_e$:$\nu_\mu\bar{\nu}_\mu$:$\nu_\tau\bar{\nu}_\tau$.

and mass squared differences are fixed to the best fit values reported in [55]. We set θ_{13} to zero, avoiding in this way possible Earth matter effects.

The total muon flux is given by the formula, see e.g. [56]:

$$\Phi_\mu = \int_{E_\mu^{\rm th}}^{m_\chi} dE_\mu \int_{E_\mu}^{m_\chi} dE_{\nu_\mu} \frac{d\phi_\nu^f}{dE_\nu} N_A R_\mu(E_\mu, E_\mu^{\rm th}) \times \left[\mathcal{N}_p \frac{d\sigma_\nu^p}{dE_\mu}(E_\nu, E_\mu) + \mathcal{N}_n \frac{d\sigma_\nu^n}{dE_\mu}(E_\nu, E_\mu) \right], \quad (45)$$

where $\mathcal{N}_p$ and $\mathcal{N}_n$ are the fractional number of protons and neutrons at the point of muon production. We consider $\mathcal{N}_p \simeq \mathcal{N}_n \simeq 0.5$, since for the through-going muons in the Super-Kamiokande detector the interaction can be assumed to occur in standard rock for which the number of protons is almost equal to the number of neutrons ($Z = 11$, $A = 22$). N_A is Avogadro's number, and the effective number of nucleons per unit volume is given by $N_A \rho_{\rm rock}$, with $\rho_{\rm rock}$ the density of the material. The muon range R_μ is defined as the distance traveled by a muon with initial energy E_μ and final energy equal to the detector energy threshold $E_\mu^{\rm th}$:

$$R_\mu(E_\mu, E_\mu^{\rm th}) = \frac{1}{\beta} \ln\left(\frac{\alpha + \beta E_\mu}{\alpha + \beta E_\mu^{\rm th}}\right), \quad (46)$$

with $\alpha \simeq 2.2 \times 10^{-3}$ GeV/(g cm^{-2}) and $\beta \simeq 4.4 \times 10^{-6}$/(g cm^{-2}). The muon energy threshold has been fixed to $E_\mu^{\rm th} = 1.6$ GeV, corresponding to the 7 m path-length cut applied on upward through-going muons in the Super-Kamiokande detector. For the differential cross sections $d\sigma_\nu^{p,n}/dE_\mu$, we use the analytic expressions for deep inelastic scattering given e.g. in Ref. [56].

Super-Kamiokande gives 90% C.L. limits on the muon flux induced by neutrinos from DM annihilations in the Sun for cones of different opening angles around the direction of the Sun [16]. To be conservative we use the limit for a cone with half-angle of 20°, which should include 90% of all muons at $m_\chi \simeq 18$ GeV [16], and a fraction approaching 100% for larger WIMP masses. The corresponding limit is $\Phi_\mu \leq 1.1 \times 10^{-14}$ cm^{-2} s^{-1} [16]. Using this upper bound on Φ_μ we obtain via Eq. (45) an upper bound on the DM scattering cross section as a function of m_χ.

These bounds are shown in Figs. 5 and 7 for the case of loop-induced WNS and WES, respectively. We show the limit for annihilations into $\tau\bar{\tau}$ and $\nu\bar{\nu}$ (assuming equal branchings into the 3 flavors). In the case of WNS, annihilations into neutrinos exclude the region compatible with DAMA, while annihilations into tau leptons might be marginally consistent with it at 3σ. In contrast, in the case of WES the neutrino bound excludes the region indicated by DAMA by more than 6 orders of magnitude. This implies that if DM couples to electrons with a cross section as large as indicated by the WES DAMA fit, cf. Eq. (42), DM annihilation into neutrinos must be very strongly suppressed. This will be hard to achieve because annihilation into charged leptons generates almost model independently also annihilation into neutrinos from W exchange at 1 loop. Thus annihilation into neutrinos is typically suppressed by a loop factor of $\mathcal{O}(10^{-4})$ compared to annihilation into charged leptons. This rules out all leptophilic DM models with dominant direct annihilation into leptons as an explanation of DAMA/LIBRA.

VII. CONCLUSIONS

In this study we have considered the hypothesis that DM has tree-level couplings only to leptons but not to quarks. Such a model has been proposed in Ref. [28] to reconcile the DAMA annual modulation signal with constraints from searches for nuclear recoils from DM scattering. Our results imply, however, that this is not possible for the following reasons:

(1) By closing the lepton legs to a loop, we obtain a coupling to the charge of the nucleus by photon exchange. Whenever the Dirac structure of the DM-lepton coupling allows such a diagram at 1 or 2 loop WIMP-nucleus scattering will dominate over the scattering rate from the direct coupling to electrons, because the latter is highly suppressed by the high momentum tail of the bound state wave function. This leads to a situation very similar to the standard WIMP case, implying the well-known tension between DAMA and the constraints from CDMS and XENON10; see Fig. 5.

(2) If the DM-lepton coupling is axial vectorlike, no loop will be induced and hence the scattering proceeds only by the interaction with electrons bound to the atoms of the detector. We have performed a careful analysis of this case, taking into account the peculiarities of scattering off electrons in bound states. We find that this model is strongly disfavored as an explanation of the DAMA signal because
   (a) the predicted spectral shape of the modulated and/or unmodulated signal in DAMA provides a very bad fit to the data as shown in Fig. 6, and
   (b) the cross section required to explain the DAMA signal is ruled out by Super-Kamiokande constraints on neutrinos from DM annihilations in the Sun; see Fig. 7.

The arguments 1 and 2(a) are rather model independent, relying only on the presence of the effective DM-lepton vertex, while the argument in 2(b) depends on the assumption that neutrinos are produced by DM annihilations. Because of $SU(2)_L$ gauge symmetry, generically one expects that DM will couple to both, charged leptons and neutrinos, which would open the annihilation channel into $\nu\bar{\nu}$. If for some reason DM couples only to charged leptons, DM would generically also annihilate into $\tau\bar{\tau}$, leading

again to the neutrino signal. In order to evade the Super-Kamiokande constraint one has to forbid the coupling of DM to neutrinos and to the tau lepton. Let us mention that the most generic way to avoid coupling to neutrinos is the chiral coupling only to right-handed leptons. Note, however, that such a chiral $V + A$ coupling involves a vector-like coupling which will induce DM-quark scattering via the loop diagram and argument 1 applies. Another way to evade the bound from annihilations would be to assume that DM is not self-conjugate and postulate the presence of a large $\chi - \bar{\chi}$ asymmetry in our halo; see e.g., Refs. [57–59].

In conclusion, we have shown that the hypothesis of DM interactions only with leptons does not provide a satisfactory solution to reconcile the DAMA annual modulation signal with constraints from other direct detection experiments.

ACKNOWLEDGMENTS

We would like to thank Alexander Merle, Thomas E. J. Underwood, and Andreas Weiler for discussions, and Nicolao Fornengo and Marco Cirelli for help in the calculation of the neutrino spectra. This work was partly supported by the Sonderforschungsbereich TR 27 of the Deutsche Forschungsgemeinschaft. J. K. received support from the Studienstiftung des Deutschen Volkes.

Noted added.—After the completion of this work we became aware of Ref. [68], where CDMS publishes constraints on electronlike events above 2 keV in their detector. These results apply to the case of axial coupling, where scattering off electron dominates. From Fig. 6 we find that our fit predicts an unmodulated rate of 0.4 (1.5) events/d/kg/keV at 2 keV if the lowest energy bin of the modulated rate is (is not) taken into account. CDMS observes 1.93 ± 0.24 events/d/kg/keV at 2 keV. Assuming a flat background in the energy range of interest an upper limit on a possible signal from DM of 0.5 events/d/kg/keV at 90% C.L. is obtained at 2 keV (see Fig. 3 of [68]). The signal in Ge is expected to be roughly 1 order of magnitude smaller than in iodine due to wave function suppression. This estimate suggests that the results of [68] do not rule out the DAMA region shown in Fig. 7. A more detailed analysis may still be of interest, though.

APPENDIX A: LOOP-INDUCED DM-QUARK INTERACTIONS

In this Appendix we calculate the cross sections for DM-nucleon scattering through the loop-induced interactions shown in Fig. 2. The main results were already collected in Sec. III B in the leading log approximation, while here we give full one-loop results and describe how the approximate two-loop results were obtained. For calculations we use the FEYNCALC package [60]. The cross section for scattering of a nonrelativistic DM particle χ with mass m_χ on a nucleus at rest carrying charge Z and having a mass m_N is

$$\frac{d\sigma}{dE_d} = \frac{\overline{|\mathcal{M}|^2}}{32\pi m_N m_\chi^2 v^2}, \tag{A1}$$

with $v \sim 10^{-3}$ the χ velocity, E_d the kinetic recoil energy of the nucleus, and $\mathcal{M}$ the matrix element for $\chi N \to \chi N$ scattering.

We start with the vector type interaction between leptons and DM, $\mathcal{L}_\ell = G(\bar{\chi}\Gamma^\mu_\chi \chi)(\bar{\ell} c^\ell_V \gamma_\mu \ell)$ with $\Gamma^\mu_\chi = (c^\chi_V + c^\chi_A \gamma_5)\gamma^\mu$; see Eq. (1). The matrix element for $\chi N \to \chi N$ scattering generated through the one-loop diagram of Fig. 2 is then

$$\begin{aligned}\mathcal{M} &= \mathcal{C}^{(1)}_V(\mu)(\bar{u}'_\chi \Gamma^\mu_\chi u_\chi)\left\langle N(p') \left| \sum_i Q_i(\bar{q}_i \gamma_\mu q_i) \right| N(p) \right\rangle \\ &= \mathcal{C}^{(1)}_V(\mu)(\bar{u}'_\chi \Gamma^\mu_\chi u_\chi) Z F(q)(\bar{u}'_N \gamma_\mu u_N).\end{aligned} \tag{A2}$$

The sum is over the light quarks q_i with charges Q_i, $F(q)$ is the nuclear form factor defined in Sec. III B, and $\mathcal{C}^{(1)}_V(\mu)$ is the one-loop factor calculated in the $\overline{\text{MS}}$ scheme

$$\begin{aligned}\mathcal{C}^{(1)}_V(\mu) = \frac{2\alpha_{\text{em}}}{\pi} G c^\ell_V \int_0^1 dx x(1-x) \\ \times \log\left[\frac{-x(1-x)q^2 + m_\ell^2 - i0}{\mu^2}\right],\end{aligned} \tag{A3}$$

where $q^2 \simeq -\kappa^2 = -2m_N E_d$ is the momentum transfer [in the calculation of the Super-Kamiokande bounds we used $q^2 \simeq -\mathcal{O}(m_\chi^2 v^2)$]. In the calculation we set $\mu = \Lambda$, with $\Lambda \sim 10$ GeV, because this is the scale at which the Wilson coefficient G is generated.[7] For $m_\ell \gg \kappa$ one can neglect the momentum transfer in the above integral, giving an approximate expression

$$\mathcal{C}^{\text{LL}}_V(\mu) = \frac{\alpha_{\text{em}}}{3\pi} G c^\ell_V \log(m_\ell^2/\mu^2), \tag{A4}$$

which is very precise for muon and tau running in the loop. It is quite precise also for the electron, even though $m_e \sim \kappa$. The reason is that there is still a hierarchy $m_e \ll \mu \simeq \Lambda$. Neglecting the difference between m_e and κ then corresponds to a leading log (LL) approximation in the renormalization group running, while the induced error is only logarithmic in $1 + \mathcal{O}(\kappa/m_e)$.

The $\chi N \to \chi N$ differential cross section $d\sigma/dE_d$ in the leading log approximation is given in Eq. (17). Multiplying it by $|\mathcal{C}^{(1)}_V/\mathcal{C}^{\text{LL}}_V|^2$ one obtains the full one-loop prediction. In

[7] This choice of μ does not minimize the size of the logarithm in $\mathcal{C}^{(1)}_V(\mu)$. However, since the expansion parameter α_{em} is small this does not invalidate the use of perturbation theory. For a choice of $\mu \ll \Lambda$ one would need to take into account renormalization group flow and mixing of operators.

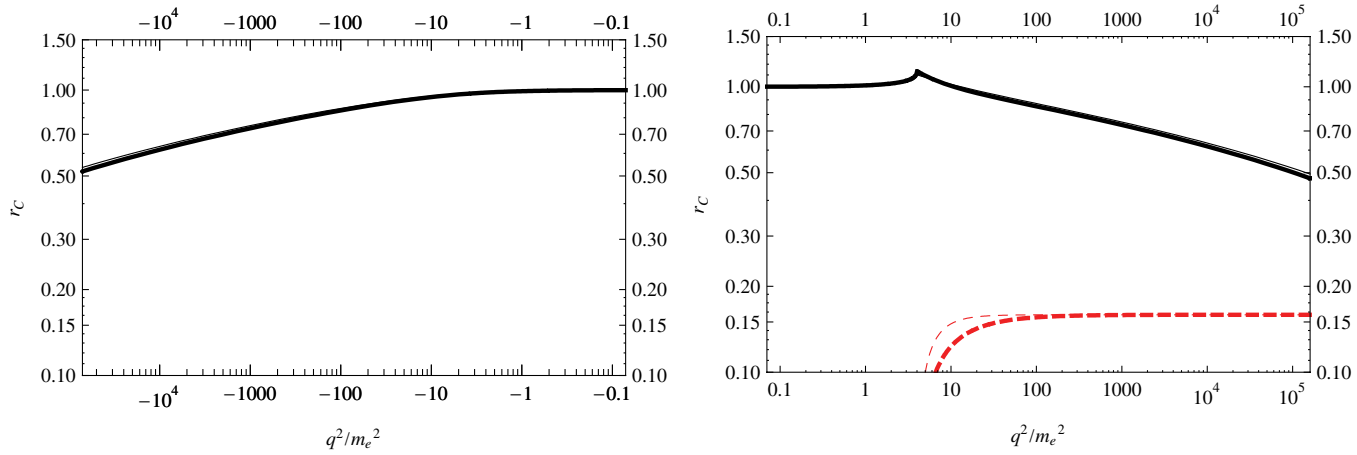

FIG. 9 (color online). The real (solid line) and imaginary (red dashed line) parts of the loop factor ratios $r_C = \mathcal{C}^{(1)}/\mathcal{C}^{\rm LL}$ as a function of q^2/m_e^2 for vector (thick lines) and tensor (thin lines) lepton currents (these two lines overlap within the precision that can still be seen on the plot). The left plot is for q^2 negative (spacelike momentum exchange), the right for q^2 positive (timelike momentum exchange). We take $m_\ell = m_e$ and $\mu = 10$ GeV.

Fig. 9 we show the value of $\mathcal{C}_V^{(1)}/\mathcal{C}_V^{\rm LL}$ for $m_\ell = m_e$ and $\mu = 10$ GeV. Note that above the pair production threshold, $q^2 > 4m_e^2$, it develops an imaginary part, since electrons in the loop can go on shell. The important thing for our purposes, though, is that $\mathcal{C}_V^{(1)}/\mathcal{C}_V^{\rm LL}$ is a slowly varying function of q^2 and is of $\mathcal{O}(1)$ in the range of spacelike $q^2 \sim -m_e^2$ of interest to us, so that the LL approximation is quite precise. Even so, in the numerical analysis in Sec. V we use the full one-loop results.

Let us next move to the tensor DM-lepton interaction, $\mathcal{L}_\ell = G(\bar\chi\Gamma_\chi^{\mu\nu}\chi)(\bar\ell\sigma_{\mu\nu}\ell)$ with $\Gamma_\chi^{\mu\nu} = (c_T + ic_{AT}\gamma_5)\sigma^{\mu\nu}$. The matrix element for $\chi N \to \chi N$ scattering is

$$\mathcal{M} = \mathcal{C}_T(\mu)(\bar u_\chi'\Gamma_\chi^{\mu\nu}u_\chi)\frac{q^\nu}{q^2}\left\langle N(p')\left|\sum_i Q_i(\bar q_i\gamma_\mu q_i)\right|N(p)\right\rangle$$
$$= \mathcal{C}_T(\mu)(\bar u_\chi'\Gamma_\chi^{\mu\nu}u_\chi)\frac{q^\nu}{q^2}ZF(q)(\bar u_N'\gamma_\mu u_N), \qquad \text{(A5)}$$

with the one-loop factor in dimensional regularization (as before the pole is to be subtracted using the $\overline{\rm MS}$ scheme)

$$\mathcal{C}_T^{(1)}(\mu) = -\frac{2\alpha_{\rm em}}{\pi}m_\ell G B_0(q^2, m^2, m^2). \qquad \text{(A6)}$$

Here $B_0(k^2, m^2, M^2)$ is a two-point scalar Veltman-Passarino function. Explicit expressions for it can be found e.g. in [61]. In the leading log approximation the above expression becomes (in the $\overline{\rm MS}$ scheme)

$$\mathcal{C}_T^{\rm LL}(\mu) = \frac{2\alpha_{\rm em}}{\pi}m_\ell G\log(m_\ell^2/\mu^2). \qquad \text{(A7)}$$

In this limit the differential scattering cross section is given in Eq. (18), while the full one-loop result is obtained by multiplying it with $|\mathcal{C}_T^{(1)}/\mathcal{C}_T^{\rm LL}|^2$. The numerical value for the ratio $\mathcal{C}_T^{(1)}/\mathcal{C}_T^{\rm LL}$ is shown in Fig. 9, obtained using the LOOPTOOLS package [62].

The scalar-type DM-lepton interaction $\mathcal{L}_{\rm eff} = G(\bar\chi\Gamma_\chi\chi)(\bar\ell c_S^\ell\ell)$ with $\Gamma_\chi = (c_S^\chi + ic_P^\chi\gamma_5)$ induces DM-quark interaction through two-loop diagrams; see Fig. 2. This contribution is relatively easy to compute in the limit of heavy leptons using the operator product expansion. First one integrates out the heavy leptons, thus matching onto the local dimension seven operator

$$\mathcal{L}_{\rm eff} = C_S(\mu)\frac{1}{m_\ell}(\bar\chi\Gamma_\chi\chi)F_{\mu\nu}F^{\mu\nu}/e^2, \qquad \text{(A8)}$$

where the Wilson coefficient is

$$C_S = \tfrac{2}{3}\alpha_{\rm em}^2 G c_S^\ell. \qquad \text{(A9)}$$

This then enters a loop with two photons attached to the nucleon current. We evaluate this one-loop diagram in the heavy nucleon limit, which gives for the matrix element

$$\mathcal{M} = \frac{C_S}{16\pi^2}\frac{2\pi^2\kappa}{m_\ell}(\bar u_\chi'\Gamma_\chi u_\chi)Z^2\tilde F(q)\left(\bar u_N'\frac{1}{2}(1+\gamma_0)u_N\right), \qquad \text{(A10)}$$

with $\kappa = \sqrt{2m_N E_d}$ the recoil three-momentum of the nucleus, and $\tilde F(q)$ the two-loop nuclear form factor. The resulting differential cross section is given in Eq. (19).

The derivation for scalar DM follows along the same lines. One matches onto the dimension 6 operator

$$\mathcal{L}_{\rm eff} = C_{S,5}(\mu)\frac{1}{m_\ell}(\chi^\dagger\chi)F_{\mu\nu}F^{\mu\nu}/e^2, \qquad \text{(A11)}$$

with the Wilson coefficient $C_{S,5} = \frac{2}{3}\alpha_{\rm em}^2 G_5 d_S^\ell$, which then gives a matrix element for χN scattering

$$\mathcal{M} = \frac{C_{S,5}}{16\pi^2}\frac{2\pi^2\kappa}{m_\ell}Z^2\tilde F(q)\left(\bar u_N'\frac{1}{2}(1+\gamma_0)u_N\right). \qquad \text{(A12)}$$

APPENDIX B: DERIVATION OF THE COUNTING RATE FOR WIMP-ELECTRON SCATTERING

Using coordinate space Feynman rules we obtain for the matrix element for WIMP scattering on an electron bound in the atomic shell with quantum numbers nlm

$$\mathcal{M}_{nlm}^{rr's s'} = G \int d^3x \psi_{nlm}(\mathbf{x}) e^{i(\mathbf{k}-\mathbf{k}'-\mathbf{p}')\mathbf{x}} \bar{u}_\chi^{r'} \Gamma_\chi^\mu u_\chi^r \bar{u}_e^s \Gamma_{e\mu} u_e^s. \tag{B1}$$

Here, $\mathbf{k}$ and $\mathbf{k}'$ are the initial and final momenta of the WIMP, and $\mathbf{p}'$ is the momentum of the electron in the final state. The momentum of the initial state bound electron is determined by momentum conservation: $\mathbf{p} \equiv \mathbf{k}' + \mathbf{p}' - \mathbf{k}$. Specializing now to the axial-vector case $\Gamma_\chi^\mu = \Gamma_e^\mu = \gamma^\mu\gamma^5$ we obtain for nonrelativistic χ and electrons[8]

$$\overline{|\mathcal{M}_{nlm}|^2} = \frac{1}{4}\sum_{rr's s'} |\mathcal{M}_{nlm}^{rr's s'}|^2 = 48 m_e^2 m_\chi^2 G^2 |\psi_{nlm}(\mathbf{p})|^2, \tag{B2}$$

where the momentum space wave function $\psi_{nlm}(\mathbf{p})$ is defined by

$$\psi_{nlm}(\mathbf{p}) = \int d^3x \psi_{nlm}(\mathbf{x}) e^{-i\mathbf{p}\mathbf{x}} \equiv \chi_{nl}(p) Y_{lm}(\theta, \phi), \tag{B3}$$

with the normalization

$$\int \frac{d^3p}{(2\pi)^3} |\psi_{nlm}(\mathbf{p})|^2 = 1. \tag{B4}$$

For the differential cross section we have

$$\frac{d\sigma_{nlm}^{\mathrm{WES}}}{dE_d} = \frac{\overline{|\mathcal{M}_{nlm}|^2}}{32\pi E_\chi E_e v_{\chi e} |\mathbf{k} + \mathbf{p}|}. \tag{B5}$$

Here, $E_\chi \approx m_\chi$, $E_e \approx m_e$ (using $E_B \ll m_e$), and $v_{\chi e}$ is the relative velocity of the WIMP and the bound electron. The event rate is obtained by summing over all shells and integrating over the electron momenta in each shell:

$$\frac{dR^{\mathrm{WES}}}{dE_d} = \frac{\rho_0 \eta_e}{m_\chi \rho_{\mathrm{det}}} \int \frac{d^3p}{(2\pi)^3} \int d^3v v_{\chi e} f_\odot(\mathbf{v}) \sum_{nlm} \frac{d\sigma_{nlm}^{\mathrm{WNS}}}{dE_d}. \tag{B6}$$

The angular dependence of the wave function disappears due to the orthogonality relation $\sum_m Y_{lm}(\theta, \phi) Y_{lm}^*(\theta, \phi) = (2l+1)/4\pi$ for the spherical harmonics. In the laboratory frame the electron and DM momentum form an angle θ, so that $\cos\theta = \mathbf{k}\mathbf{p}/kp$. For the integration over $\cos\theta$ from the d^3p integral we have to take into account Eq. (29), which holds under the approximation $E_d \ll m_e \leq E_e \ll m_\chi$ and implies

$$\cos\theta \approx -\frac{1}{v}\left(\frac{E_d}{p} + \frac{p}{2m_\chi}\right). \tag{B7}$$

The leading order corrections to this expression give the kinematically available range for $\cos\theta$:

$$(\cos\theta)_{\max} - (\cos\theta)_{\min} \approx \frac{1}{m_\chi v p}\sqrt{2m_e(E_d - E_B)(m_\chi^2 v^2 - 2m_\chi E_d)}. \tag{B8}$$

Then, $|\mathbf{k} + \mathbf{p}| \approx \sqrt{m_\chi^2 v^2 - 2m_\chi E_d}$, and Eq. (B6) leads to the expression for the counting rate given in Eq. (30). The approximations we have made in deriving the formulas are accurate up to about 10% for $m_\chi \sim 1$ GeV, but the error decreases with increasing m_χ, and we estimate an accuracy of $\mathcal{O}(1\%)$ for $m_\chi \gtrsim 100$ GeV.

APPENDIX C: NUMERICAL EVALUATION OF ATOMIC MATRIX ELEMENTS

In this Appendix, we describe how we compute the radial momentum space wave function $\chi(p)$ for WIMP-electron inelastic scattering and the matrix elements $\langle n'l'm'|e^{i(\mathbf{k}-\mathbf{k}')\mathbf{x}}|nlm\rangle$ defined in Eq. (37) for WIMP-atom elastic and inelastic scattering.

WIMP-electron scattering: The momentum space radial wave function $\chi_{nl}(p)$, see Eq. (B3), required for the evaluation of the event rate for WES, is obtained by splitting the coordinate space wave function $\psi_{nlm}(\mathbf{x})$ into its angular part $Y_{lm}(\theta, \phi)$ and its radial part $R_{nl}(r)$, and computing

$$\begin{aligned}\chi_{nl}(p) &= \frac{4\pi}{2l+1}\sum_m \psi_{nlm}(\mathbf{p}) Y_{lm}(\theta_p, \phi_p) \\ &= 2\pi \int dr r^2 R_{nl}(r) \int d(\cos\theta) P_l(\cos\theta) e^{ipr\cos\theta} \\ &= 4\pi i^l \int dr r^2 R_{nl}(r) j_l(pr).\end{aligned} \tag{C1}$$

Here, $\mathbf{p}$ is a momentum space vector with modulus p and arbitrary orientation (θ_p, ϕ_p), and $P_l(\cos\theta)$ is a Legendre polynomial. In the second line, we have used the orthogonality of the spherical harmonics, and in the third line, we have used Gegenbauer's formula [63], which relates the Fourier type integral over a Legendre polynomial to the spherical Bessel function of the same degree.

The radial wave functions $R_{nl}(r)$ can be approximated by a linear combination of so-called Slater type orbitals [64]:

$$R_{nl}(r) = \sum_k c_{nlk} \frac{(2Z_{lk})^{n_{lk}+1/2}}{a_0^{3/2}\sqrt{(2n_{lk})!}} (r/a_0)^{n_{lk}-1} \exp(-Z_{lk} r/a_0). \tag{C2}$$

[8] Using hydrogenlike atom approximation we estimate the relativistic corrections to be of order 20% for electrons from the $1s$ shell of iodine and smaller for the other shells.

Here, a_0 is the Bohr radius, and the parameters c_{nlk}, n_{lk}, and Z_{lk} are taken from [64].

With $R_{nl}(r)$ given in the form of Eq. (C2), we can evaluate (C1) analytically, which gives

$$\chi_{nl}(p) = \sum_k c_{nlk} 2^{-l+n_{lk}} \left(\frac{2\pi a_0}{Z_{lk}}\right)^{3/2} \left(\frac{ipa_0}{Z_{lk}}\right)^l \frac{(1+n_{lk}+l)!}{\sqrt{(2n_{lk})!}} {}_2F_1\left[\frac{1}{2}(2+l+n_{lk}), \frac{1}{2}(3+l+n_{lk}), \frac{3}{2}+l, -\left(\frac{pa_0}{Z_{lk}}\right)^2\right], \quad \text{(C3)}$$

with ${}_2F_1(a, b, c, x)$ being a hypergeometric function.

WIMP-atom elastic scattering: The matrix element for this case can be written as

$$\sum_m \langle nlm|e^{i(\mathbf{k}-\mathbf{k}')\mathbf{x}}|nlm\rangle = \sum_m \int dr d\Omega r^2 [R_{nl}(r)]^2 Y^*_{lm}(\theta, \phi) Y_{lm}(\theta, \phi) e^{iKr\cos\theta} \quad \text{(C4)}$$

$$= (2l+1) \int dr r^2 [R_{nl}(r)]^2 \frac{\sin Kr}{Kr} \quad \text{(C5)}$$

with the abbreviation $K \equiv |\mathbf{K}| \equiv |\mathbf{k} - \mathbf{k}'|$. This integral has the form of a Fourier sine transform, and can be evaluated efficiently using the fast Fourier transform algorithm. For $R_{nl}(r)$, we use again the expansion Eq. (C2), with the coefficients taken from [64].

WIMP-atom inelastic scattering: Here the numerical evaluation of the atomic matrix elements is slightly more involved than for el-WAS because now $\psi_{n'l'm'}(\mathbf{x}) \neq \psi_{nlm}(\mathbf{x})$. We expand the factor $e^{i\mathbf{Kx}}$ in Eq. (37) in spherical harmonics [65] and rewrite the angular integral over a product of three spherical harmonics in terms of the Wigner-3j symbols [66]. This gives

$$\langle n'l'm'|e^{i\mathbf{Kx}}|nlm\rangle = 4\pi \int dr r^2 R_{nl}(r) R_{n'l'}(r) \sum_{L,M} j_L(Kr) Y_{LM}(\theta_K, \phi_K) \frac{(-1)^m}{\sqrt{4\pi}} \sqrt{(2l+1)(2l'+1)(2L+1)} \times \begin{pmatrix} l & l' & L \\ 0 & 0 & 0 \end{pmatrix} \begin{pmatrix} l & l' & L \\ m & m' & M \end{pmatrix}, \quad \text{(C6)}$$

where j_L denotes a spherical Bessel function of the first kind, and θ_K, ϕ_K are the angular components of $\mathbf{K}$. To compute the cross section, we need the expression

$$\sum_{mm'} |\langle n'l'm'|e^{i\mathbf{Kx}}|nlm\rangle|^2 = (2l+1)(2l'+1) \sum_L (2L+1) \left[\begin{pmatrix} l & l' & L \\ 0 & 0 & 0 \end{pmatrix}\right]^2 \left[\int dr r^2 R_{nl}(r) R_{n'l'}(r) j_L(Kr)\right]^2. \quad \text{(C7)}$$

Here, we have used the symmetry and orthogonality relations of the Wigner-3j symbols and of the spherical harmonics. The expression in the second set of square brackets has the form of a spherical Bessel transform, which we evaluate by using an algorithm due to Sharafeddin *et al.* [67], based on rewriting the spherical Bessel function as a

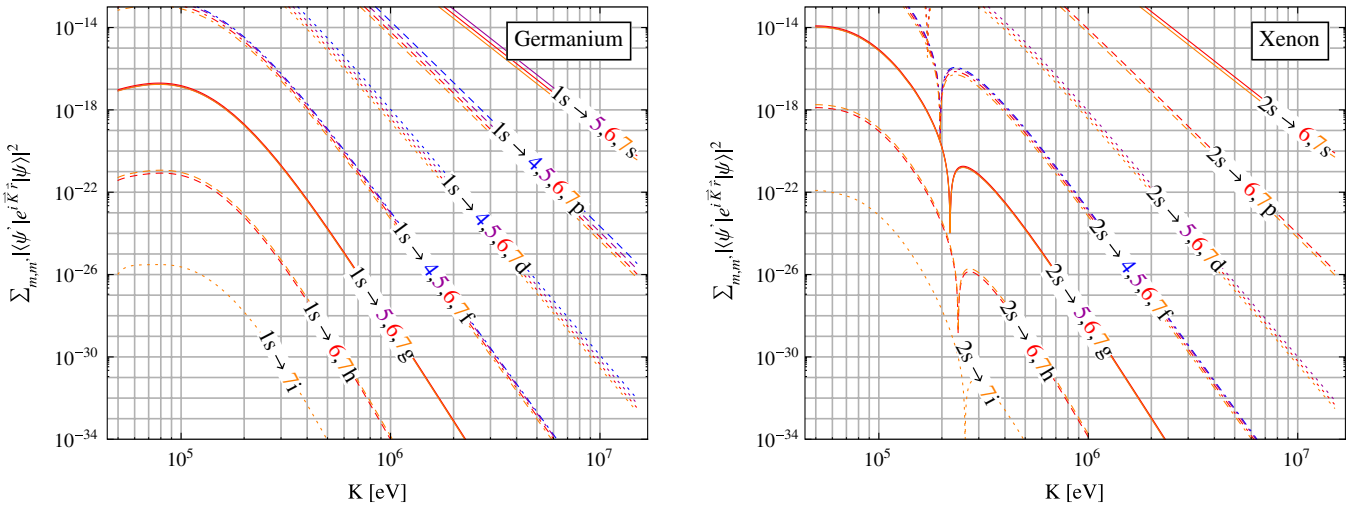

FIG. 10 (color online). A few examples for ie-WAS matrix elements of germanium and xenon. The plot shows transitions from the 1*s*, respectively, 2*s* orbitals to some of the lowest unoccupied states.

finite Fourier series, thus converting the integral to a sum of Fourier sine and Fourier cosine transforms. The initial state wave functions R_{nl} are again given by Eq. (C2) and Ref. [64], while for the final state wave functions $R_{n'l'}$, we use the hydrogenlike approximation (with an effective charge $Z = 3$ due to screening of the nuclear charge by inner electrons) since accurate tabulated wave functions for excited atoms were not available. Also, we consider only transitions from the $1s$, $2s$, and $3s$ levels to the first two unoccupied s shells; we have checked numerically that these transitions are the most important ones. Figure 10 shows some of the ie-WAS matrix elements for germanium and xenon. We find that for germanium (xenon) transitions from the $1s$ ($2s$) orbital dominate. Our approximations should correctly reproduce the qualitative behavior of the matrix elements at large momentum transfer and should lead to a good order of magnitude estimate of the ie-WAS event rate.

APPENDIX D: ON THE EQUILIBRIUM OF DM CAPTURE AND ANNIHILATIONS IN THE SUN

In the calculation of the neutrino flux from DM annihilations in the Sun we have assumed that WIMP captures and annihilations are in equilibrium, which makes the result independent of the DM annihilation cross section $\langle\sigma_{\rm ann}v\rangle$. Here we comment on the validity of this assumption. Let us first estimate the cutoff scale Λ for the effective theory description of the DM-lepton coupling. For the two examples of $V\otimes V$ and $A\otimes A$ couplings, the neutrino bounds are of order $\sigma^0_{\chi e}\sim 10^{-43}$ cm^2 and 10^{-38} cm^2, respectively; see Figs. 5 and 7. From Eq. (13) we can estimate the corresponding cutoff scales as $\Lambda_V\sim 100$ GeV and $\Lambda_A\sim 10$ GeV, where we took coupling constants c_i^χ to be of order $\mathcal{O}(1)$. In DM annihilations the four-momentum transfer squared is of order m_χ^2. For $m_\chi\sim 10$ GeV, relevant for WNS, the WIMP annihilations may then also be described by effective field theory. Using effective interactions in Eq. (1) (extending them to neutrinos), we find

$$\text{vector: } \langle\sigma_{\rm ann}v\rangle\sim\frac{G^2m_\chi^2}{\pi}=\sigma^0_{\chi e}\frac{m_\chi^2}{m_e^2}\sim 10^{-24}\ \text{cm}^3\,\text{s}^{-1}\left(\frac{\sigma^0_{\chi e}}{10^{-43}\ \text{cm}^2}\right)\left(\frac{m_\chi}{10\ \text{GeV}}\right)^2. \tag{D1}$$

In the WES case, however, the effective theory typically cannot be applied since the momentum transfer for annihilations is above the cutoff scale. Therefore, in general we cannot make model independent statements about $\langle\sigma_{\rm ann}v\rangle$ without specifying the UV completion of the effective $\chi\ell$ vertex. An order of magnitude estimate can still be obtained from dimensional analysis as

$$\text{axial: } \langle\sigma_{\rm ann}v\rangle\sim\frac{g^4}{m_\chi^2}\sim 10^{-21}\ \text{cm}^3\,\text{s}^{-1}\times g^4\left(\frac{m_\chi}{100\ \text{GeV}}\right)^{-2}, \tag{D2}$$

with g a typical coupling constant between leptons and the dark sector.

Equilibrium of WIMP capture and annihilations is obtained if $\tanh^2(t_\odot/\tau)$ is close to 1; see Eq. (43). Figure 11 shows the values of $\langle\sigma_{\rm ann}v\rangle$ for which $t_\odot/\tau = 1$ and 5 as a function of m_χ. The values of scattering cross sections $\sigma^0_{\chi e}$ for $V\otimes V$ and $A\otimes A$ Lorentz structures were chosen to be above (but close to) the Super-Kamiokande bounds shown in Figs. 5 and 7. Since $\tanh^2 x\approx 1$ for $x\gtrsim 5$, WIMP capture and annihilations are in equilibrium in the Sun for values of $\langle\sigma_{\rm ann}v\rangle$ above the curve for $t_\odot/\tau = 5$. Comparing Eqs. (D1) and (D2) with the ranges shown in the figure we conclude that the assumption of equilibrium is very well justified in the cases of our interest.

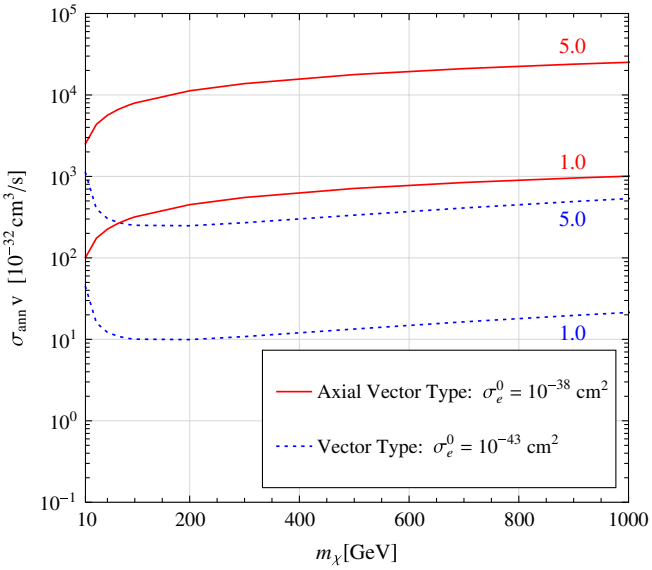

FIG. 11 (color online). Contours of $t_\odot/\tau = 5$ and $t_\odot/\tau = 1$; see Eq. (43). For the case of vector (axial-vector) coupling we have used a scattering cross section of $\sigma^0_{\chi e} = G^2m_e^2/\pi = 10^{-43}(10^{-38})$ cm^2, motivated by the results of the Super-Kamiokande bound. For values of $\langle\sigma_{\rm ann}v\rangle$ above the curve for $t_\odot/\tau = 5$, WIMP capture and annihilations are in equilibrium in the Sun.

[1] R. Bernabei *et al.*, Riv. Nuovo Cimento Soc. Ital. Fis. **26N1**, 1 (2003).
[2] R. Bernabei *et al.* (DAMA Collaboration), Eur. Phys. J. C **56**, 333 (2008).
[3] Z. Ahmed *et al.* (CDMS Collaboration), Phys. Rev. Lett. **102**, 011301 (2009).
[4] J. Angle *et al.* (XENON Collaboration), Phys. Rev. Lett. **100**, 021303 (2008).
[5] A. Bottino, F. Donato, N. Fornengo, and S. Scopel, Phys. Rev. D **77**, 015002 (2008).
[6] A. Bottino, F. Donato, N. Fornengo, and S. Scopel, Phys. Rev. D **78**, 083520 (2008).
[7] F. Petriello and K. M. Zurek, J. High Energy Phys. 09 (2008) 047.
[8] J. L. Feng, J. Kumar, and L. E. Strigari, Phys. Lett. B **670**, 37 (2008).
[9] S. Chang, A. Pierce, and N. Weiner, Phys. Rev. D **79**, 115011 (2009).
[10] M. Fairbairn and T. Schwetz, J. Cosmol. Astropart. Phys. 01 (2009) 037.
[11] C. Savage, G. Gelmini, P. Gondolo, and K. Freese, J. Cosmol. Astropart. Phys. 04 (2009) 010.
[12] Y. G. Kim and S. Shin, arXiv:0901.2609.
[13] E. Behnke *et al.* (COUPP Collaboration), Science **319**, 933 (2008).
[14] H. S. Lee *et al.* (KIMS Collaboration), Phys. Rev. Lett. **99**, 091301 (2007).
[15] S. Archambault *et al.*, arXiv:0907.0307.
[16] S. Desai *et al.* (Super-Kamiokande Collaboration), Phys. Rev. D **70**, 083523 (2004).
[17] D. Hooper, F. Petriello, K. M. Zurek, and M. Kamionkowski, Phys. Rev. D **79**, 015010 (2009).
[18] D. Tucker-Smith and N. Weiner, Phys. Rev. D **64**, 043502 (2001).
[19] S. Chang, G. D. Kribs, D. Tucker-Smith, and N. Weiner, Phys. Rev. D **79**, 043513 (2009).
[20] J. March-Russell, C. McCabe, and M. McCullough, J. High Energy Phys. 05 (2009) 071.
[21] Y. Cui, D. E. Morrissey, D. Poland, and L. Randall, J. High Energy Phys. 05 (2009) 076.
[22] C. Arina, F.-S. Ling, and M. H. G. Tytgat, arXiv: 0907.0430.
[23] K. Schmidt-Hoberg and M. W. Winkler, arXiv:0907.3940.
[24] G. Angloher *et al.* (CRESST-II Collaboration), Astropart. Phys. **31**, 270 (2009).
[25] D. B. Cline, W. Ooi, and H. Wang, arXiv:0906.4119.
[26] R. Foot, Phys. Rev. D **78**, 043529 (2008).
[27] E. Masso, S. Mohanty, and S. Rao, Phys. Rev. D **80**, 036009 (2009).
[28] R. Bernabei *et al.*, Phys. Rev. D **77**, 023506 (2008).
[29] A. Dedes, I. Giomataris, K. Suxho, and J. D. Vergados, arXiv:0907.0758.
[30] O. Adriani *et al.* (PAMELA Collaboration), Nature (London) **458**, 607 (2009).
[31] J. Chang *et al.*, Nature (London) **456**, 362 (2008).
[32] A. A. Abdo *et al.* (Fermi LAT Collaboration), Phys. Rev. Lett. **102**, 181101 (2009).
[33] P. J. Fox and E. Poppitz, Phys. Rev. D **79**, 083528 (2009).
[34] Q.-H. Cao, E. Ma, and G. Shaughnessy, Phys. Lett. B **673**, 152 (2009).
[35] A. Ibarra, A. Ringwald, D. Tran, and C. Weniger, J. Cosmol. Astropart. Phys. 08 (2009) 017.
[36] G. Jungman, M. Kamionkowski, and K. Griest, Phys. Rep. **267**, 195 (1996).
[37] R. Bernabei *et al.*, Phys. Lett. B **389**, 757 (1996).
[38] E. M. Drobyshevski, Mod. Phys. Lett. A **23**, 3077 (2008).
[39] R. Bernabei *et al.*, Eur. Phys. J. C **53**, 205 (2008).
[40] J. Graichen, K. Maier, J. Schuth, A. Siepe, and W. von Witsch, Nucl. Instrum. Methods Phys. Res., Sect. A **485**, 774 (2002).
[41] J. A. Bearden and A. F. Burr, Rev. Mod. Phys. **39**, 125 (1967).
[42] P. Gondolo and G. Gelmini, Phys. Rev. D **71**, 123520 (2005).
[43] P. Fayet, Phys. Rev. D **75**, 115017 (2007).
[44] M. Ackermann *et al.* (AMANDA Collaboration), Astropart. Phys. **24**, 459 (2006).
[45] A. Achterberg *et al.* (IceCube Collaboration), Astropart. Phys. **26**, 155 (2006).
[46] R. Abbasi, Phys. Rev. Lett. **102**, 201302 (2009).
[47] J. L. Feng, J. Kumar, J. Learned, and L. E. Strigari, arXiv:0808.4151.
[48] A. Gould, Astrophys. J. **321**, 571 (1987).
[49] J. N. Bahcall, A. M. Serenelli, and S. Basu, Astrophys. J. **621**, L85 (2005).
[50] A. Gould, Astrophys. J. **321**, 560 (1987).
[51] A. H. G. Peter, Phys. Rev. D **79**, 103532 (2009).
[52] S. Ritz and D. Seckel, Nucl. Phys. **B304**, 877 (1988).
[53] M. Cirelli *et al.*, Nucl. Phys. **B727**, 99 (2005).
[54] M. Blennow, J. Edsjo, and T. Ohlsson, J. Cosmol. Astropart. Phys. 01 (2008) 021.
[55] T. Schwetz, M. Tortola, and J. W. F. Valle, New J. Phys. **10**, 113011 (2008).
[56] V. Barger, W.-Y. Keung, G. Shaughnessy, and A. Tregre, Phys. Rev. D **76**, 095008 (2007).
[57] S. Nussinov, Phys. Lett. **165B**, 55 (1985).
[58] S. M. Barr, R. S. Chivukula, and E. Farhi, Phys. Lett. B **241**, 387 (1990).
[59] D. B. Kaplan, Phys. Rev. Lett. **68**, 741 (1992).
[60] R. Mertig, M. Bohm, and A. Denner, Comput. Phys. Commun. **64**, 345 (1991).
[61] G. 't Hooft and M. J. G. Veltman, Nucl. Phys. **B153**, 365 (1979).
[62] T. Hahn and M. Perez-Victoria, Comput. Phys. Commun. **118**, 153 (1999).
[63] M. Abramowitz and I. A. Stegun, *Handbook of Mathematical Functions with Formulas, Graphs, and Mathematical Tables* (Dover, New York, 1964), ninth Dover printing, tenth GPO printing ed., ISBN 0-486-61272-4.
[64] C. F. Bunge, J. A. Barrientos, and A. V. Bunge, At. Data Nucl. Data Tables **53**, 113 (1993).
[65] J. D. Jackson, *Classical Electrodynamics* (Wiley, New York, 1998), 3rd ed., Vol. 2009.
[66] J. J. Sakurai, *Modern Quantum Mechanics* (Addison-Wesley, Reading, MA, 1994), 2nd ed..
[67] O. A. Sharafeddin, H. F. Bowen, D. J. Kouri, and D. K. Hoffman, J. Comput. Phys. **100**, 294 (1992).
[68] Z. Ahmed *et al.* (CDMS Collaboration), arXiv:0907.1438.